THEORETICAL STUDY OF THE EARTHQUAKE RESPONSE OF THE PARADISE COOLING TOWER

Prepared by

T.Y. Yang, C.S. Gran, and J.L. Bogdanoff
School of Aeronautics and Astronautics
Purdue University
West Lafayette, Indiana

Submitted to

THE NATIONAL SCIENCE FOUNDATION

April 3, 1978

50272-101

REPORT DOCUMENTATION PAGE	1. REPORT NO. NSF/RA-780526	2.	3. Recipient's Accession No. PB292504

4. Title and Subtitle
Theoretical Study of the Earthquake Response of the Paradise Tower

5. Report Date
April 3, 1978

6.

7. Author(s)
T.Y. Yang, C.S. Gran, J.L. Bogdanoff

8. Performing Organization Rept. No.

9. Performing Organization Name and Address
Purdue University
School of Aeronautics and Astronautics
West Lafayette, Indiana 47907

10. Project/Task/Work Unit No.

11. Contract(C) or Grant(G) No.
(C)
(G) ENV7401575

12. Sponsoring Organization Name and Address
Applied Science and Research Applications (ASRA)
National Science Foundation
1800 G Street, N.W.
Washington, D.C. 20550

13. Type of Report & Period Covered

14.

15. Supplementary Notes

16. Abstract (Limit: 200 words)

Since the use of cooling towers is increasing over the use of once-through water cooling systems, and since many of these towers are being built in regions of high seismic risk, their dynamic behavior has received considerable attention. In this study, quadrilateral plate finite elements and beam finite elements, both oriented arbitrarily in 3-dimensional space, are used in the analysis of the dynamic behavior of cooling towers. It is found that such a model will accurately predict natural frequencies and mode shapes. It also provides a realistic modeling of the base support system, important in the prediction of displacements and stresses in the base region. A model of a cooling tower in the TVA's 1200 MW fossil fuel steam generating plant in Paradise, Kentucky is used in the study. The report describes the system, its finite elements, methods of analysis, assumptions, evaluative analysis, and free vibration analysis of the Paradise Cooling Tower.

17. Document Analysis a. Descriptors

Cooling towers
Fossil fuels
Earthquake resistant construction
Dynamic structural analysis
Models
Kentucky
Earthquakes

b. Identifiers/Open-Ended Terms
TVA

c. COSATI Field/Group

18. Availability Statement	19. Security Class (This Report)	21. No. of Pages
NTIS		65
	20. Security Class (This Page)	22. Price PC A04 MF A01

THEORETICAL STUDY OF THE EARTHQUAKE RESPONSE OF THE PARADISE COOLING TOWER

Prepared by

T.Y. Yang, C.S. Gran, and J.L. Bogdanoff
School of Aeronautics and Astronautics
Purdue University
West Lafayette, Indiana

Submitted to

THE NATIONAL SCIENCE FOUNDATION

April 3, 1978

TABLE OF CONTENTS

INTRODUCTION

The increasing size of modern electricity generating power plants has brought about tremendous requirements for cooling water. Present once-through cooling systems are proving to be inadequate for several reasons. Growing public opposition to thermal pollution incurred by discharging into natural bodies of water, increasingly stringent regulations applied to waste water, and the decreasing availability of suitable sites are paramount concerns. The use of cooling towers resolves these difficulties.

Natural draught cooling towers are hyperbolic shells of revolution in form, supported upon a system of closely-spaced, inclined columns. These shells are usually made of reinforced concrete of variable thickness and are stiffened at the top and base by geometric variations which may be considered essentially as ring beams. Monumental structures, both in size and cost, cooling towers perform a vital service in the operation of a large power plant.

The dynamic behavior of cooling towers has received considerable attention. The spectacular collapse of several towers at Ferrybridge, England in 1965 demonstrated their vulnerability to severe wind loading [Ref. 1]. Now cooling towers are being built in regions of high seismic risk. Anticipating the varying design criteria of different geographic locations has led to an investigation of the seismic response of cooling towers.

Early dynamic analyses of cooling towers were conducted for the case of a shell with fixed base. The methods of analysis include numerical

integration [Ref. 2], finite difference [Ref. 3], and the finite element method with the use of rotational ring-type shell elements [Ref. 4]. In reality, however, the cooling towers are supported by discrete columns. These supports provide a condition of physical restraint that is significantly different than the conventional fixed or simply-supported boundary conditions. The effect of discrete column supports must be taken into account if the behaviors of the cooling towers are to be correctly predicted. Efforts to include such effects were made for both static and dynamic cases in, among other references, References 5 and 6, by the use of curved rotational shell finite elements. The discrete columns in both of these references were modeled by a rotational shell element for which the stiffness and mass properties are equivalent to those of the discrete columns.

If the finite element method is chosen to analyze the cooling towers, the most exact way to model the supporting columns appears to be modeling each column as a distinct element through the use of column finite elements with an exact stiffness formulation. To accomplish this, however, one cannot use the rotational shell finite elements since the nodal circles cannot be connected to the column joints. Quadrilateral or triangular shell finite elements must be used instead. In this study, quadrilateral elements are used to model the cooling tower shell. Each quadrilateral element in the bottom ring is subdivided into three triangular elements to provide an extra nodal point along the base circumference at which another pair of columns may be attached.

The capability of the quadrilateral shell finite elements in predicting natural frequencies of cooling towers is first evaluated through an example of a fixed-base cooling tower. Results for frequencies compared well with previously reported results [Refs. 2-4]. The capability

of the column finite elements in modeling the discrete column supports is then evaluated through free vibration analysis of an example of a cooling tower with column supports. Results for frequencies also compared well with a previous alternative solution [Ref. 6].

The two types of finite elements are finally used to model a cooling tower in Unit #3 of the Tennessee Valley Authority's 1200 MW fossil fuel steam generating power plant at Paradise, Kentucky, U.S.A. Natural frequencies and mode shapes are determined. The modal superposition method is used to find the tower's time-history response of displacements when subjected to the North-South acceleration component of the 1940 El Centro earthquake record for a period of 30 seconds. It is found that only those modes with one circumferential wave are responsive to the horizontal earthquake disturbance. A response spectrum analysis is used to find the maximum displacements and stresses in the structure with an assumed damping coefficient of four percent. The effect of variations in assumed damping coefficient is also considered.

The most critical region is found to be in the supporting columns. These inclined supports provide resistance to the overturning moment and base shear primarily by means of axial forces. This particular facet of the total structure must be accurately included in the analytical model if meaningful results are to be obtained. The forces and bending moments in the base region of the shell, particularly at the joints to the columns, are critical. However, with the increased thickness and reinforcement, the resulting stresses can be kept within tolerable limits, as is the case with the present tower.

DESCRIPTION OF THE SYSTEM

There are three cooling towers in the Paradise steam generating plant. The reinforced concrete cooling tower is in the form of a hyperbolic shell of revolution as shown in Fig. 1. The shell thickness varies from 24 inches at the base to 7 inches at the throat and then to 9 inches at the top. The cylinder strength f'_c of the concrete is 4000 psi at 28 days. The tower is supported by 40 pairs of reinforced concrete columns of circular cross sections, with f'_c of 5000 psi. Each pair has a concrete footing buried in the excavated limestone rock. The top of the tower is stiffened by a reinforced concrete ring of rectangular cross section. The top of the ring provides a walk way. All reinforcement is new billet steel, ASTM A432.

Due to the axisymmetrical nature of the design, both the circumferential and meridional reinforcements vary only along the meridional direction and remain constant along the circumferential direction. The distribution of the equivalent modulus of elasticity for the circumferential reinforcements along the meridional direction, presented in Fig. 2, is calculated from the design drawings. The distribution of the equivalent modulus of elasticity for the meridional reinforcements along the meridian is presented in Fig. 3. Panels A, B, and C indicate three slightly different types of arrangements in reinforcements in the lower part of the shell.

FINITE ELEMENTS

Two types of finite elements are used in the modeling of the cooling tower: a three dimensional beam finite element and an orthotropic quadrilateral flat plate finite element oriented arbitrarily in the three

dimensional space. The former is used to model the discrete supporting columns and the ring beam at the top of the shell. The latter is used to model the hyperboloidal shell of revolution.

The three dimensional beam finite element has two nodal points, each of which has six degrees of freedom: three displacement degrees of freedom in the three Cartesian coordinate directions and three rotational degrees of freedom about the three Cartesian coordinate axes, respectively [Ref. 7]. The stiffness matrix is derived on the basis that the axial displacement varies linearly along the element and the transverse deflection varies cubically along the element. The mass matrix is formulated on the basis of lumped masses.

The three dimensional orthotropic quadrilateral plate element is shown in Fig. 4. This element has five degrees of freedom $\bar{u}$, $\bar{v}$, and $\bar{w}$ in the Cartesian local coordinate directions $\bar{x}$, $\bar{y}$, and $\bar{z}$, respectively; and two slope degrees of freedom about the $\bar{x}$ and $\bar{y}$ axes, respectively. For reasons of computational efficiency, the quadrilateral element is composed of four triangular elements. The four triangles share a common central nodal point which is located at the average of the coordinates of the four corner nodal points. The five degrees of freedom at this central nodal point are eliminated at the elemental level prior to assemblage. Thus the quadrilateral element effectively has a total of 20 degrees of freedom, five per nodal point.

The membrane stiffness of each sub-triangular element is represented by the constant strain based on linear displacement functions in both $\bar{u}$ and $\bar{v}$ [Ref. 8]. The flexural stiffness of each sub-triangular element is represented by the fully compatible HCT element based on the cubic displacement functions in $\bar{w}$ [Ref. 9]. The orthotropic material property is

included in the formulations for both the membrane and flexural stiffness matrices. The mass matrix of the quadrilateral element is formulated on the basis of lumped masses. The formulation, with reference to the local coordinates $\bar{x}$, $\bar{y}$, and $\bar{z}$, is given in the following symbolic form

$$\underset{20x1}{\{\bar{F}\}} = \underset{20x20}{[k]} \quad \underset{20x1}{\{\bar{q}\}} + \underset{20x20}{[m]} \quad \underset{20x1}{\{\ddot{\bar{q}}\}} \qquad (1)$$

where $\{\bar{F}\}$ and $\{\bar{q}\}$ are vectors of nodal forces and displacements, respectively; [k] and [m] are the element stiffness and mass matrices, respectively; the "dot" represents time derivative, and the "bar" represents local coordinates.

Through a congruent coordinate transformation technique, the element formulation (1) in local coordinates is transformed into the formulation in global coordinates,

$$\underset{24x1}{\{F\}} = \underset{24x24}{[T]^T} \underset{20x20}{[k]} \underset{20x24}{[T]} \underset{24x1}{\{q\}} - \underset{24x20}{[T]^T} \underset{20x20}{[m]} \underset{20x24}{[T]} \underset{24x1}{\{\ddot{q}\}} \qquad (2)$$

where the matrix [T] is the coordinate transformation matrix. This coordinate transformation generates six degrees of freedom at each nodal point: three displacement degrees of freedom u, v, and w in the global coordinate directions, x, y, and z, respectively; and three rotational degrees of freedom θ_x, θ_y, and θ_z about the x, y, and z axes, respectively. Formulation (2) for each individual element can thus be used in the three dimensional space to model shell structures.

METHOD OF ANALYSIS

The dynamic earthquake response of the subject cooling tower is determined by means of modal analysis. The equations of motion of the N

degree-of-freedom discrete system are uncoupled by means of a linear coordinate transformation. This transformation if obtained by assuming that the response is a superposition of the N normal modes of the system multiplied by corresponding time-dependent generalized coordinates. Thus, the dynamic analysis consists of the following steps: 1) determine the natural vibration mode shapes and frequencies which depend on the inertia and stiffness properties of the system; 2) calculate the dynamic response of each mode and superimpose them to find the total response. The second step is accomplished by two different techniques. The modal superposition method is used to determine the time-history response and the response spectrum method approximates the maximum response.

Free Vibration Analysis

The equations of motion for an elastic system with a finite number of degrees of freedom undergoing free oscillations may be written in matrix form as

$$[M] \{\ddot{q}(t)\} + [K] \{q(t)\} = \{0\} \tag{3}$$

where [M] and [K] are positive definite global inertia and stiffness matrices, respectively. If damping forces are assumed to be proportional to the inertia and/or the elastic forces, they will have no effect on the mode shapes.

Since free oscillations are harmonic in time, the N degrees of freedom $\{q\}$ in any mode r may be expressed

$$\{q_r\} = \{\phi_r\} \sin \omega_r t \quad , \quad r = 1, 2, \ldots, N \tag{4}$$

in which $\{\phi\}$ is the vector of amplitudes of $\{q\}$ and ω is the circular natural frequency. Substituting Eqn. (4) into Eqn. (3) yields

$$[[K] - \omega_r^2 [M]] \{\phi_r\} = \{0\} \ . \tag{5}$$

A non-trivial solution for $\{\phi\}$ is possible only if the determinant of Eqn. (5) vanishes,

$$|[K] - \omega^2[M]| = 0. \tag{6}$$

The above determinant is an N^{th} order equation in ω^2. The N roots or eigenvalues ω^2 are the squares of the natural frequencies of vibration of the structure. Corresponding to each ω_r is an eigenvector $\{\phi_r\}$ which gives the associated free vibration mode shape.

Two methods are used to solve for the eigenvalues and eigenvectors of the characteristic determinant. The first, the subspace iteration method [Ref. 10], is used to determine the lowest p roots. The inverse power method with shifts [Ref. 11] is used to determine p eigenvalues within a specified frequency range.

Completion of the eigenvalue problem yields the desired transformation or modal matrix $[\Phi]$ consisting of the N columns of orthogonal eigenvectors $\{\phi\}$ which will uncouple the system of equations. The modes $\{\phi\}$ are customarily normalized so that

$$\{\phi\}^T[M]\{\phi\} = 1.$$

The independent equations of motion resemble the equations of a single-degree-of-freedom system. Each normal mode may now be treated as an independent one-degree-of-freedom system.

Time-History Response by Modal Superposition

The equations of motion of an elastic viscously damped structure with support motion and no external forces can be written as

$$[M]\{\ddot{q}\} + [C]\{\dot{q}\} + [K]\{q\} = -[M]\{\ddot{x}\} \tag{7}$$

where $\{q(t)\}$ = the vector of displacements of the mass with respect to the support

$[C]$ = damping matrix

$\{\ddot{x}(t)\}$ = the vector of support accelerations.

Assuming damping is a linear combination of inertia and stiffness, the modal matrix can be used as a linear transformation to uncouple these equations, that is

$$\{q(t)\} = [\Phi]\{n(t)\} \tag{8}$$

with

$$[\Phi]^T[M][\Phi] = [I]$$

and

$$[\Phi]^T[K][\Phi] = [\Omega^2]$$

where $[I]$ is the identity matrix and $[\Omega^2]$ is a diagonal matrix of eigenvalues ω^2. Introducing the notation

$$[\Phi]^T[C][\Phi] = [2\zeta\omega],$$

substituting Eqn. (8) into Eqn. (7), and premultiplying by $[\Phi]^T$ yields equations of the form

$$\ddot{n}(t) + 2\zeta_r\omega_r\dot{n}(t) + \Omega_r{}^2 n(t) = N_r(t), \qquad r = 1, 2, \ldots, n \tag{9}$$

where $\{N\} = -[\Phi]^T[M]\{\ddot{x}\}$ are generalized forces and ζ_r is the critical damping coefficient of the r^{th} mode.

The solution of Eqn. (9) can be readily obtained by means of the Laplace transformation. If there is no initial displacement or velocity.

$$\eta_r(t) = \frac{1}{\omega_r'} \int_0^t N_r(\tau) \exp[-\zeta_r \omega_r (t-\tau)] \sin[\omega_r' (t-\tau)] d\tau \qquad (10)$$

where $\omega_r' = \omega_r \sqrt{1-\zeta_r}$ is the damped natural frequency.

If the modes were not initially normalized with respect to mass, Eqn. (10) may be written as

$$\eta_r(t) = -\frac{\Gamma_r}{\omega_r'} \int_0^t \ddot{x}(\tau) \exp[-\zeta_r \omega_r (t-\tau)] \sin[\omega_r' (t-\tau)] d\tau \qquad (11)$$

where $\Gamma_r = \dfrac{\sum_{i=1}^{n} M_i \phi_{ir}}{\sum_{i=1}^{n} M_i \phi_{ir}^2}$ is the modal participation factor.

If there is no damping, the modal response becomes

$$\eta_r(t) = -\frac{\Gamma_r}{\omega_r} \int_0^t \ddot{x}(\tau) \sin \omega_r (t-\tau) d\tau . \qquad (12)$$

The total response of the structure at any time t may be obtained by adding together the individual modal responses at that time. This superposition is given by Eqn. (8).

Response Spectrum Analysis

Inspection of Eqn. (11) clearly shows the response to be dependent upon the magnitude of the Duhamel's integral. Yet when damping is included, exact evaluation of this integral at every time is extremely tedious. It is therefore of interest to construct curves that represent maximum numerical values of the responses as functions of the critical damping ratio and the structure's natural frequency or natural period for

a given excitation. Housner, et. al. [Ref. 12] have evaluated such maxima for all earthquakes from which reliable records have been obtained. The maximum modal responses are presented in the form of spectral acceleration, $S_{a_r}\{\omega_r, \zeta_r\ t)$ vs. period, where

$$S_{a_r} = \left[\omega_r \int_0^t \ddot{x}(\tau) \exp[-\zeta_r \omega_r (t-\tau)] \sin[\omega_r' (t-\tau)] d\tau \right]_{max} \qquad (13)$$

This pseudoacceleration is of great importance because the maximum individual modal responses can be computed directly from it [Ref. 13]. From Eqns. (11) and (13) it is clear that

$$\eta_{r_{max}} = -\frac{\Gamma_r}{\omega_r^2} S_{a_r}. \qquad (14)$$

It should be noted that statistically the pseudoacceleration is always smaller than or equal to max $|\ddot{x}|$ because it neglects the part of $\ddot{x}$ whose product by M would produce a force in the damper, but its use is justified by considerations of simplicity.

Root Mean Square (RMS) Technique

Individual maximum modal responses are computed from the response spectrum analysis. Maximum displacements of the r^{th} mode are

$$\{q_r\}_{max} = \{\phi_r\}\eta_{r_{max}}. \qquad (15)$$

However the maximum displacement of every mode does not occur simultaneously, therefore the total maximum response cannot be obtained by merely superimposing the individual modal maxima. It has been shown that the most probably value of any earthquake response quantity is given by the

square root of the sum of the squares of the corresponding modal maxima [Ref. 14]. Thus, the estimated total maximum response of the n^{th} degree of freedom, $q'_{n_{max}}$, is

$$q'_{n_{max}} = [\sum_{r=1}^{N} q_{nr}]^{\frac{1}{2}}. \tag{16}$$

ASSUMPTIONS

The following assumptions underlie this study:

(1) Since the column footings are imbedded in limestone rock, the bases of the supporting columns are assumed to be fixed.

(2) The reinforced concrete cooling tower behaves elastically.

(3) The shell material is orthotropic. Moduli of elasticity are different in the circumferential and longitudinal directions.

EVALUATIVE ANALYSIS

In order to substantiate the reliability of the results obtained through the use of the present beam and quadrilateral plate elements, it is necessary to compare their performance with that of alternative methods. This is accomplished by means of two examples for which frequencies have been previously determined using various techniques. The first example is one in which the base of the hyperboloidal shell is fixed; the second has "discrete" supporting columns.

Free Vibration Analysis of an Example of a Cooling Tower with Fixed Base

The first example is described in Fig. 5. The isotropic modulus of elasticity of the reinforced concrete cooling tower is 3×10^{6} psi, the Poisson's ratio is 0.15, and the mass density is 0.225×10^{-3} lbs-sec^2/in^4. The base of the tower is assumed to be rigidly fixed. This example was

analyzed previously be Carter, et. al. [Ref. 2] using numerical integration technique; by Hashish and Abu-Sitta [Ref. 3] using finite difference technique, and by Sen and Gould [Ref. 4] using curved rotational shell finite elements. Their results for the natural frequencies are shown in Table I.

In this study, three different finite element meshes are used: 4x16 (number of meridional shell elements x number of circumferential shell elements), 6x20, and 8x20, the three meshes correspond to 384, 720, and 960 degrees of freedom, respectively. The present results are shown in Table I for comparison. It is seen that for the 4x16 mesh, the frequencies are, in general, higher than those from the alternative solutions [Refs. 2-4]. These discrepancies are, however, within tolerable range from a practical engineering point of view. For the 6x20 mesh, the frequencies, in general, reduce slightly. For the 8x20 mesh, the frequencies reduce further and are in close agreement with those from the previous solutions. The mode shapes are also in good agreement with the alternative predictions. It may reasonably be concluded from this example that the quadrilateral elements are adequate for the dynamic analysis of cooling towers with fixed base.

Free Vibration Analysis of an Example of a Cooling Tower with Discrete Supporting Columns

An example of a concrete cooling tower with discrete supporting columns has been treated by Gould et. al. [Ref. 6] with the use of curved rotational shell finite elements. The supporting columns were modeled by a special rotational elastic element whose stiffness and mass properties are equivalent to those of the discrete columns. This element has the same degrees of freedom at the nodal circles as those assumed in

the shell element. The free stress states between column joints were modified by applying a system of self-equilibriated edge loadings to the base of the shell.

The example is described in Fig. 6. The cooling tower has 88 supporting columns with cross sectional area of 52 by 24 square inches. For the concrete in both the shell and the columns, the modulus of elasticity, the Poisson's ratio, and the mass density were assumed to be 4×10^{6} psi, 1/6, and 0.225×10^{-3} lbs-sec^2/in^4, respectively.

In Ref. 6, the cooling tower was first analyzed with the base fixed and then with the base supported by the "equivalent" columns. Part of the results for natural frequencies are shown in Table II.

For the case of fixed base, the present results obtained by the use of 8x20 mesh (960 degrees of freedom) agree reasonably well with those obtained by Gould et. al. using 14 rotational shell finite elements. For the case with discrete supporting columns, the present results obtained by the use of 8x22 mesh (1320 degrees of freedom) are, in general, lower than those obtained by Gould et. al. (See Table II). This may imply that the present realistic column modeling provides a less stiff representation than the equivalent rotational shell element.

For the modeling with 8x22 mesh, the lowest row is modeled by 66 triangular elements instead of 22 quadrilateral elements. Each initially quadrilateral element is divided into three triangular elements with two nodes on the top and three nodes at the bottom. By doing so, 44 nodes are created which can be connected to the top joints of the 44 pairs of column finite elements.

The successful completion of the first two examples provides assurance that the combined usage of sufficient numbers of quadrilateral shell

elements and beam elements will quite accurately predict the dynamic behavior of column supported cooling towers. The cooling tower in the Paradise Steam Generating Plant is then analyzed in this manner.

FREE VIBRATION ANALYSIS OF THE PARADISE COOLING TOWER

Lowest Frequency Vibration Modes

In the preliminary free vibration analysis of the Paradise cooling tower, three different quadrilateral shell element modelings are used: 4x16 mesh, 6x20 mesh, and 8x20 mesh, respectively. The first modeling has 16 beam finite elements at the top of the shell to represent the stiffened ring beam. The other two modelings use 20 stiffened beam elements for this purpose. In the three modelings, each quadrilateral element in the base row is divided into three triangular elements so that it has three nodal points at the base line. Thus for the 6x20 and 8x20 meshes, the base circle of the tower has 40 nodes that can be connected to the 40 pairs of discrete column elements. For the 4x16 mesh, the 40 pairs of columns are replaced by 32 pairs of equivalent columns. The three modelings thus have 576, 960, and 1200 degrees of freedom, respectively.

Since the arrangement of the reinforcements in the circumferential direction is different than that in the meridional direction, each quadrilateral shell finite element must be orthotropic. The distributions of the equivalent moduli of elasticity in the circumferential and meridional directions are shown in Figs. 2 and 3, respectively. The moduli of elasticity used for the orthotropic quadrilateral shell elements are based on these distributions.

The present results for the natural frequencies of several modes using different meshes are given in Table III. The first two meridional mode shapes for the third through seventh circumferential modes are shown in Fig. 7. It is seen that the base of the shell moves considerably due to the flexible nature of the column supports. This phenomenon cannot be predicted if the base of the shell is assumed as fixed. Figure 7 also shows the meridional mode shapes for the hypothetical case in which the base of the shell is fixed. It is interesting to see the manner in which the flexible column supports affect the meridional mode shapes.

It is important to point out that when the circumferential mode number is equal to one, the shell vibrates in a side-swaying type of motion. When the circumferential mode number is not equal to one, the shell vibrates in a breathing type of motion. Previous studies [Refs. 6 and 15] have pointed out that only the modes with one circumferential wave are excitable by the horizontal earthquake motion. Thus, the side-swaying or eccentric modes are of primary importance in the study of earthquake response. And the column supports drastically influence the frequencies of these modes, reducing the fundamental eccentric frequency by as much as 50% [Ref. 16].

Eccentric Modes with Refined Modeling

The preliminary stages of this investigation require comparative testing of the present modeling against several alternative solution methods. This involves finding the lowest natural frequency vibration modes which are breathing modes. It is found that modeling only a portion of the axisymmetric structure will not adequately reproduce these mode shapes, most probably due to the difficulties encountered in

prescribing boundary conditions for a doubly-curved surface. The full-shell model avoids such difficulties and produces accurate results for all the vibration modes computed.

In the analysis of the cooling tower's response to horizontal earthquake excitation, only those modes with one circumferential wave are of interest. These eccentric modes can be accurately predicted by using a finite element model of only half of the actual shell surface. With such an idealization the element mesh may be refined, which is greatly beneficial in determining the stress field. And the number of degrees of freedom associated with the problem is reduced from a comparable full shell model.

Several different half-shell mesh configurations are used to model the Paradise cooling tower. These element mesh sizes include: 4x10 (345 D.O.F.), 8x10 (573 D.O.F.), 9x10 (654 D.O.F.) and 9x10 (918 D.O.F.). The 918 D.O.F. model differs from the others in that it uses two beam finite elements to represent each individual supporting column except for the column at one edge of the half-shell ($\theta = 0°$). This particular column is formed by six beam elements in order to find detailed stress information along the column length. Again, all the above models feature beam elements to form the top ring-beam of the shell, orthortopic quadrilateral plate elements with the triangular variation at the base to form the shell and the beam elements to form the discrete column supports. The 9x10 half-shell model is shown in Fig. 8.

The first three eccentric frequencies are calculated using the half-shell modeling as shown in Fig. 8. Results are presented in Table IV. Comparison with the eccentric frequencies presented in Table III for the 4x16 full shell (which in half shell form would have 288 D.O.F.) indicates

good corroboration. The slight discrepancy,particularly in the first mode stems from the inadequacy of the 32 "equivalent" pairs of columns in simulating the action of the 40 actual pairs. Any aberrations within the convergence pattern of the frequencies of the half-shell models are likely to be caused by the extreme sensitivity of frequencies to changes in meridional curvature as reported by several authors (e.g. Ref. 3) and confirmed in the present study.

Mode shapes are found using the most sophisticated 9x10 model with 918 degrees of freedom. The meridional shapes of the first three eccentric modes are shown in Figs. 9, 10,and 11. The circumferential shape of all three modes remains circular throughout the body of the shell. However, the discrete supporting columns affect this shape at the shell base. A number of waves equal to one-half the number of column pairs are found to exist in both the transverse and in-plane directions. The deviation this phenomena produces is slight in the first eccentric mode, practically non-existant in the second mode and pronounced in the third. The circumferential mode shapes at the base of the shell are shown in Figs. 12, 13, and 14 for the first, second,and third eccentric modes, respectively. Although the third eccentric mode shows the wavy distributions of both meridional and radial displacements at the base of the shell, they are not of primary concern simply because the earthquake response of the cooling tower is dominated by the first mode with a slight contribution from the second mode.

EARTHQUAKE RESPONSE OF THE PARADISE COOLING TOWER

Earthquake Disturbance

Previous studies have indicated that only one horizontal component of an earthquake is sufficient for design of a hyperbolic cooling tower [Ref. 16]. In this study, the North-South acceleration component of the 1940 El Centro earthquake is used to model the ground motion. This is one of the most severe earthquakes of record with a maximum peak horizontal ground acceleration of 0.33g where g is the acceleration due to gravity. A record of this acceleration component is shown in Fig. 15 for a period of 30 seconds. The record was obtained from known values of acceleration at 1500 equally spaced points. Interpolation is accomplished by assuming the curve to be linear in the intervals. Values of spectral acceleration computed from this data show good agreement with those obtained by Housner et. al. [Ref. 12].

Time History Response

A preliminary investigation of the seismic response of the Paradise cooling tower is carried out using the 4x16 mesh full-shell model with 576 degrees of freedom. The time-history response for deflections obtained in an analysis which includes the first eccentric mode and all lower breathing modes is compared to a similar analysis in which only the first eccentric mode is included. The two responses are practically identical, confirming the findings of previous authors [Refs. 6 and 10] that only those modes with one circumferential wave are excitable by horizontal earthquake motion.

In these analyses, the Duhamel's integral is evaluated first at 1500 equally spaced time steps over the 30 second period and then at 15000 steps. Results are in excellent agreement. The integration time step Δt must be chosen so that

$$\frac{\Delta t}{T} < 0.1$$

where T is the period of the highest frequency mode retained in the analysis. Failure to satisfy this condition will effectively filter out the participation of the higher modes [Ref. 10].

The 9x10 half-shell model with 918 degrees of freedom is now used to determine the time history of deflections. The North-South acceleration component of the 1940 El Centro earthquake is applied parallel to the plane of symmetry. The first three eccentric modes of vibration are included, each with damping assumed to be zero.

The response at the tip of the shell at $\theta = 0°$, where θ is defined as the circumferential angle measured from the diameter that coincides with the direction of the earthquake, is shown in Fig. 16. The maximum deflection is found to be 8.43 inches, arriving at 11.48 seconds. The maximum peak to peak deflection is 16.67 inches from 11.48 to 11.68 seconds. The response for the deflections at the top of the column at $\theta = 0°$ is shown in Fig. 17. The maximum deflection is 3.78 inches at 10.56 seconds, with the maximum peak to peak displacement being 6.65 inches from 10.36 to 10.56 seconds. Although these deflections are smaller than those at the shell tip, they are still considerable and should not be neglected as in the case of assuming the shell base to be fixed.

The radial deflection shapes along a meridian at $\theta = 0°$ are shown in Fig. 18 for the two critical instances. The corresponding circumferential shapes remain circular throughout the shell. It is only at the shell base that the effect of the discrete column supports produces a slight wavy distribution of displacements during the response.

Response Spectrum Analysis

The maximum individual modal responses of the first three eccentric modes are computed by the response spectrum method. The longitudinal deflection shapes at $\theta = 0°$ are presented in Fig. 19 for the undamped case and again in Fig. 20 for the case in which a critical damping coefficient of 4% has been assumed for each mode. The response of the third mode has been magnified ten times to distinguish its shape.

Figures 19 and 20 illustrate the rapidly diminishing effect of the higher modes upon the total response. In the undamped case, the first mode contributes approximately 90% of the total, while the second and third modes contribute 9% and 1%, respectively. When 4% damping is included, the first mode accounts for over 96% of the total response, the second mode adds approximately 4%,and the third mode's contribution is negligible. Also of particular interest is the inclusion of 4% viscous damping decreases the maximum deflections by approximately 60%.

The three modal responses with 4% damping are combined by the RMS technique to determine the total maximum response of the Paradise cooling tower subjected to the El Centro earthquake. This state of deflection is enforced in a static analysis to find the maximum forces and stresses produced in the shell and columns. The contribution of gravity loading is included.

Forces and Stresses in the Shell and Columns

The longitudinal distribution of meridional and circumferential bending moment in the shell at $\theta = 0°$ are shown in Figs. 21 and 22, respectively. It is interesting to see that approximately 35 feet above the base of the shell, the moments become nearly zero which indicates predominantly membrane behavior. The maximum meridional bending moment

is 10,500 ft-lbs/ft which produces a maximum compressive bending stress of 100 psi in the concrete and a maximum tensile bending stress of 540 psi in the reinforcing bar. These stresses are computed at the shell base, mid-way between column tops where reinforcement is a minimum. The maximum circumferential bending moment is 1,330 ft-lbs/ft which produces no significant stresses in this heavily-reinforced, thick section.

The distribution of meridional membrane force at $\theta = 180°$ is shown in Fig. 23. The maximum stress resultant of 90 kips/ft at a height of 90 feet above the shell base produces a stress of 840 psi in the concrete. On the tension side ($\theta = 0°$), the maximum meridional membrane force is 40 kips/ft which produces a 5 ksi stress in the reinforcing bar. The difference between the membrane forces at $\theta = 0°$ and $\theta = 180°$ at the same height are primarily due to the dead weight of the tower.

The longitudinal distribution of circumferential membrane force at $\theta = 0°$ is shown in Fig. 24. The maximum force is 27 kips/ft at the shell base. This produces a maximum compressive stress of 80 psi in the concrete. At $\theta = 180°$, the circumferential membrane force is 6 kips/ft, producing a stress of 125 psi in the reinforcing bar.

Although the shell portion of the cooling tower could experience severe cracking and still function adequately, it appears that under the present conditions the shell will persevere with no damage.

Previous studies have concluded that the axial forces in the columns play a crucial role in determining the cooling towers response [Refs. 17 and 18]. The axial forces developed in this study are presented in Fig. 25 for each column around half of the base circumference. The maximum compressive axial force along with the associated bending moment produce a maximum stress of 5250 psi in the concrete at the middle of the column length.

The maximum stresses in the concrete at the column top and base are 4500 psi and 5145 psi, respectively. The contributions of shear and torque in the column are negligible. The maximum tensile axial force and corresponding bending moment produce a maximum stress in the high-strength reinforcement of 77.1 ksi, occurring in a cracked section at the column base. At the top and middle of the cracked column, the maximum steel stresses are 52.7 ksi and 67.6 ksi, respectively.

With the columns driven beyond the yield point, it appears evident that inelastic behavior will result. Such behavior will increase both the flexibility and the damping of the structure to a degree dependent upon the columns ductility. These alterations can be accounted for by a reduction of the design load as suggested in Ref. 19.

Effect of Viscous Damping

Since the viscous damping coefficients for the Paradise cooling tower are not known, only assumed values are used in this study. The tower is modeled by the 4x16 full-shell mesh with 576 degrees of freedom. The first eccentric mode and all lower breathing modes are included in a time-history analysis. It is assumed that all the modes have the same viscous damping coefficient. Three different values of damping coefficient are assumed for this cooling tower: 4, 7, and 10 percent of the critical value.

The ratio between the maximum shell tip deflection with damping and the maximum undamped tip deflection is plotted versus assumed critical damping coefficient in Fig. 26. Included in this figure is the maximum column top deflection ratio versus damping coefficient. The two curves are almost identical. The variations of both the maximum axial force ratio in the column at $\theta = 0°$ and the maximum bending moment ratio at

the column top versus damping coefficient are found to follow curves nearly identical to those of Fig. 26.

CONCLUSIONS

In this study, quadrilateral plate finite elements and beam finite elements, both oriented arbitrarily in three-dimensional space, are used in the analysis of the dynamic behavior of cooling towers. It is found that such a model will accurately predict natural frequencies and mode shapes. It also provides a realistic modeling of the base support system which is of utmost importance in the prediction of displacements and stresses in the base region.

Only those modes with one circumferential wave are excitable by horizontal earthquake motion. These eccentric modes can be determined with the use of a half-shell model. In this study, the contributions of the higher eccentric modes to the total deflection rapidly diminish. In the undamped case, the first mode contributes approximately 90% of the total deflection while the second and third modes contribute 9% and 1%, respectively. When damping of 4% of the critical value is included, the first mode accounts for over 96% of the total response, with the second mode adding approximately 4%,and the third mode's contribution is negligible.

Consideration must be given to the effect of the discrete supporting columns in order to accurately analyze the seismic response of cooling towers. The column supports considerably reduce the natural frequencies of a cooling tower originally assumed to have a fixed base. The tops of

the columns deflect substantially during earthquake excitation. The columns are found to be the vulnerable region in the system. In particular, the axial force in the columns appears to be the most critical.

The response of the cooling tower shell is characterized by predominantly membrane behavior. Bending is restricted to a narrow band at the base of the shell. The height of this band is less than approximately 9% of the overall height of the shell for the case studied.

For the present cooling tower, the inclusion of viscous damping with four percent of its critical value reduces the maximum displacements and stresses by about 60 percent. An increase in damping beyond this further reduces the response but to a lesser extent.

The 9x10 element mesh with 918 degrees of freedom is practically sufficient for the purpose of predicting the dynamic behavior of the cooling tower. For more detailed stress predictions, however, a finer mesh size or more sophisticated shell finite elements would be needed. Also, inelastic deformations, which may affect the dynamic behavior, have not been considered.

REFERENCES

[1] General Electricity Generating Board, "Report of the Committee of Inquiry into Collapse of Cooling Towers at Ferrybridge," November 1, 1965, Her Majesty's Stationary Office, London.

[2] Carter, R.L., Robinson, A.R., and Schnobrick, W.C., "Free Vibration of Hyperboloidal Shells of Revolution," Journal of the Engineering Mechanics Division, Proceedings of ASCE, Vol. 95, No. EM5, Oct., 1969, pp. 1033-1052.

[3] Hashish, M.G. and Abu-Sitta, "Free Vibration of Hyperbolic Cooling Towers," Journal of the Engineering Mechanics Division, Proceedings of ASCE, Vol. 97, No. EM2, April, 1971, pp. 253-269.

[4] Sen, S.K. and Gould, P.L., "Free Vibration of Shells of Revolution," Journal of the Engineering Mechanics Division, Proceedings of ASCE, Vol. 100, No. EM2, April, 1974, pp. 283-303.

[5] Sen, S.K. and Gould, P.L., "Hyperboloidal Shells on Discrete Supports," Journal of the Structural Division, Proceedings of ASCE, Vol. 99, No. ST3, March, 1973, pp. 595-603.

[6] Gould, P.L., Sen, S.K., and Suryoutomo, H., "Dynamic Analysis of Column Supported Hyperboloidal Shells," Earthquake Engineering and Structural Dynamics, Vol. 2, 1974, pp. 269-279.

[7] Przemieniecki, J.S., Theory of Matrix Structural Analysis, McGraw-Hill, New York, 1968.

[8] Turner, M.J., et al, "Stiffness and Deflection Analysis of Complex Structures," Journal of Aeronautical Sciences, Vol. 23, No. 9, Sept., 1956, pp. 805-823.

[9] Clough, R.W. and Tocher, J.L., "Finite Element Stiffness Matrices for the Analysis of Plate Bending," Proceedings of the Conference on Matrix Methods in Structural Mechanics, Air Force Flight Dynamics Lab. Report TR-66-80., Dayton, Ohio, Oct., 1965.

[10] Bathe, K.J., Wilson, E.L. and Peterson, F.P., "Structural Analysis Program (SAPIV) Manual," University of California, Berkeley, CA.

[11] Butler, T.G., et al., "The NASTRAN Manuals," NASA SP-220, March, 1976.

[12] Housner, G.W., Martel, R.R., and Alford, J.L., "Spectrum Analysis of Strong-Motion Earthquakes," Bulletin of the Seismological Society of America, Vol. 43, No. 2, April, 1953, pp. 97-119.

[13] Clough, R.W., "Earthquake Analysis by Response Spectrum Superposition," Bulletin of the Seismological Society of America, Vol. 52, No. 3, July, 1962, pp. 647-660.

[14] Goodman, L.E., Rosenblueth, E., and Newmark, N.M., "Aseismic Design of Firmly Founded Elastic Structures," ASCE Transactions, Vol. 120, 1955, pp. 782-802.

[15] Abu-Sitta, S.H. and Davenport, A.G., "Earthquake Design of Cooling Towers," Journal of the Structural Division, Proceedings of ASCE, Vol. 96, No. ST9, Sept., 1970, pp. 1889-1902.

[16] Gupla, A.K., and Schnobrick, W.C., "Seismic Analysis and Design of Hyperbolic Cooling Towers," Nuclear Engineering and Design, Vol. 36, 1976, pp. 251-260.

[17] Schnobrick, W.C. and Bupla, A.K., "Design of Cooling Towers to Resist Earthquakes," Department of Civil Engineering, University of Illinois, Urbana.

[18] Gould, P.L., et al., "Seismic Analysis of Hyperbolic Cooling Towers by the Response Spectrum Method," International Symposium on Earthquake Structural Mechanics, St. Louis, MO, August, 1976.

[19] Newmark, N.M. and Rosenblueth, Fundamentals of Earthquake Engineering, Prentice-Hall, 1971.

Table I. The Natural Frequencies (in Hz.) for a Cooling Tower with Base Fixed.

Circumferential Mode	Longitudinal Mode	Carter et al. (numerical integration)	Hashish and Abu-Sitta (finite difference)	Sen and Gould (curved rotational shell elements)	Quadrilateral finite elements		
					4x16 Mesh	6x20 Mesh	8x20 Mesh
1	1	3.2884	3.3345	3.2910	3.3119		
	2	6.7405	6.8816	6.8176	7.1638		
	3	10.5207	10.5316	10.6666	11.3170		
2	1	1.7654	1.7848	1.7662	1.8681	1.8153	
	2	3.6931	3.7234	3.6960			
	3	6.9562	6.9553	7.0058			
3	1	1.3749	1.3929		1.5356	1.4528	1.3627
	2	1.9904	2.0150		2.0969		
	3	4.3254	4.3353				
4	1	1.1808	1.2003	1.1820	1.3830	1.3248	1.2099
	2	1.4475	1.4597	1.4491	1.6136	1.5648	1.4468
	3	2.7777	2.7762	2.7866	2.8882		
5	1	1.0348	1.0441	1.0354	1.2447	1.1808	1.0556
	2	1.4293	1.4417	1.4345	1.5855	1.5806	
	3	2.0559	2.0555	2.0640	2.3176		
6	1	1.1467	1.1544		1.3120	1.2672	1.1382
	2	1.3231	1.3335		1.5492	1.5461	
	3	2.0141	2.0152		2.1702		
7	1	1.3014	1.3055		1.4460	1.4556	1.3230
	2	1.5133	1.5189		1.6040	1.6220	
	3	1.9217	1.9200		2.1470	2.0705	

Table II. The Natural Frequencies (in Hz) for a Cooling Tower with Discrete Column Supports.

Circumferential Mode	Longitudinal Mode	Fixed Base		Column Base	
		Gould et al.	This study 8x20 Mesh	Gould et al.	This Study 8x22 Mesh
3	1	1.194	1.185	1.086	1.092
	2	1.672		1.314	
4	1	1.104	1.125	0.945	0.951
	2	1.302	1.304	1.204	1.168
5	1	1.131	1.146	1.032	1.024
	2	1.453	1.463	1.256	1.219
6	1	1.400	1.405	2.235	1.189
	2	1.568		1.455	

Table III. The Natural Frequencies in Hz. for the Subject Cooling Tower

Circumferential Mode	Longitudinal Mode	4x16 Mesh	6x20 Mesh	8x20 Mesh
1	1	2.1758		
	2	3.9758		
	3	7.7884		
2	1	1.2538	1.2391	1.2148
	2	1.9882		
3	1	0.8875	0.8777	0.8857
	2	1.6263	1.5321	1.4504
4	1	0.9851	0.9306	0.9057
	2	1.3965	1.3592	1.3353
5	1	0.8446	0.8255	0.8491
	2	2.0430		
6	1	1.0235	1.0763	1.0351
	2	1.9160	1.6691	
7	1	1.2708	1.4156	1.2997
	2	1.9363	1.7525	

Table IV. Natural Frequencies (Hz) of Modes with One Circumferential Wave for the Paradise Cooling Tower.

Longitudinal Mode	Element Mesh (D.O.F.)			
	4x10 (345)	8x10 (573)	9x10 (654)	9x10 (918)
1	2.1952	2.1924	2.1962	2.1850
2	3.8723	3.6612	3.6438	3.6377
3	7.8041	7.6335	7.7131	7.6755

FIGURE CAPTIONS

Fig. 1. The Hyperbolic Cooling Tower in the TVA Steam Generating Power Plant, Unit #3, Paradise, Kentucky.

Fig. 2. The Distribution of Equivalent Modulus of Elasticity for the Circumferential Reinforcements Along the Meridional Direction.

Fig. 3. The Distribution of Equivalent Modulus of Elasticity for the Meridional Reinforcements Along the Meridional Direction.

Fig. 4. A Quadrilateral Plate Finite Element in the Three-Dimensional Space.

Fig. 5. An Example of a Reinforced Concrete Cooling Tower with Base Fixed.

Fig. 6. An Example of a Reinforced Concrete Cooling Tower with Discrete Column Supports.

Fig. 7. The Radial Deflection of a Meridional Line for Several Modes of the Paradise Cooling Tower (j = Circumferential Mode Number, m = meridional mode number).

Fig. 8. The Finite Element Modeling of the Paradise Cooling Tower (9 x 10 Half-Shell Model with Two Beam Elements Per Column).

Fig. 9. The Radial Deflection of a Meridional Line in the First Eccentric Mode of the Paradise Cooling Tower.

Fig. 10. The Radial Deflection of a Meridional Line in the Second Eccentric Mode.

Fig. 11. The Radial Deflection of a Meridional Line in the Third Eccentric Mode.

Fig. 12. The Circumferential Deflection at the Shell Base of the First Eccentric Mode.

Fig. 13. The Circumferential Deflection at the Shell Base of the Second Eccentric Mode.

Fig. 14. The Circumferential Deflection at the Shell Base of the Third Eccentric Mode.

Fig. 15. The North-South Acceleration Component of the 1940 El Centro Earthquake.

Fig. 16. The Time-History Response of Shell Tip Deflection at $\theta = 0°$ for the Undamped Case.

Fig. 17. The Time-History Response of Column Top Deflection at $\theta = 0°$ for the Undamped Case.

Fig. 18. The Radial Deflection of the Meridional Line at $\theta = 0°$ at the Time of Maximum Shell Tip Deflection ($t = 11.48$ seconds) and the Time of Maximum Column Top Deflection ($t = 10.56$ seconds).

Fig. 19. Maximum Individual Undamped Radial Deflections of the First Three Eccentric Modes from the Spectral Analysis (with the Third Mode Magnified Ten Times).

Fig. 20. Maximum Individual Radial Deflections of the First Three Eccentric Modes with Four Percent Damping from the Spectral Analysis (with the Third Mode Magnified Ten Times).

Fig. 21. Longitudinal Distribution of Meridional Bending Moment at $\theta = 0°$.

Fig. 22. Longitudinal Distribution of Circumferential Bending Moment at $\theta = 0°$.

Fig. 23. Longitudinal Distribution of Meridional Membrane Force at $\theta = 180°$.

Fig. 24. Longitudinal Distribution of Circumferential Membrane Force at $\theta = 0°$.

Fig. 25. Average Axial Force in the Supporting Columns.

Fig. 26. Variations of Maximum Tip Deflection Ratio and Maximum Column Top Deflection Ratio versus Damping Coefficient.

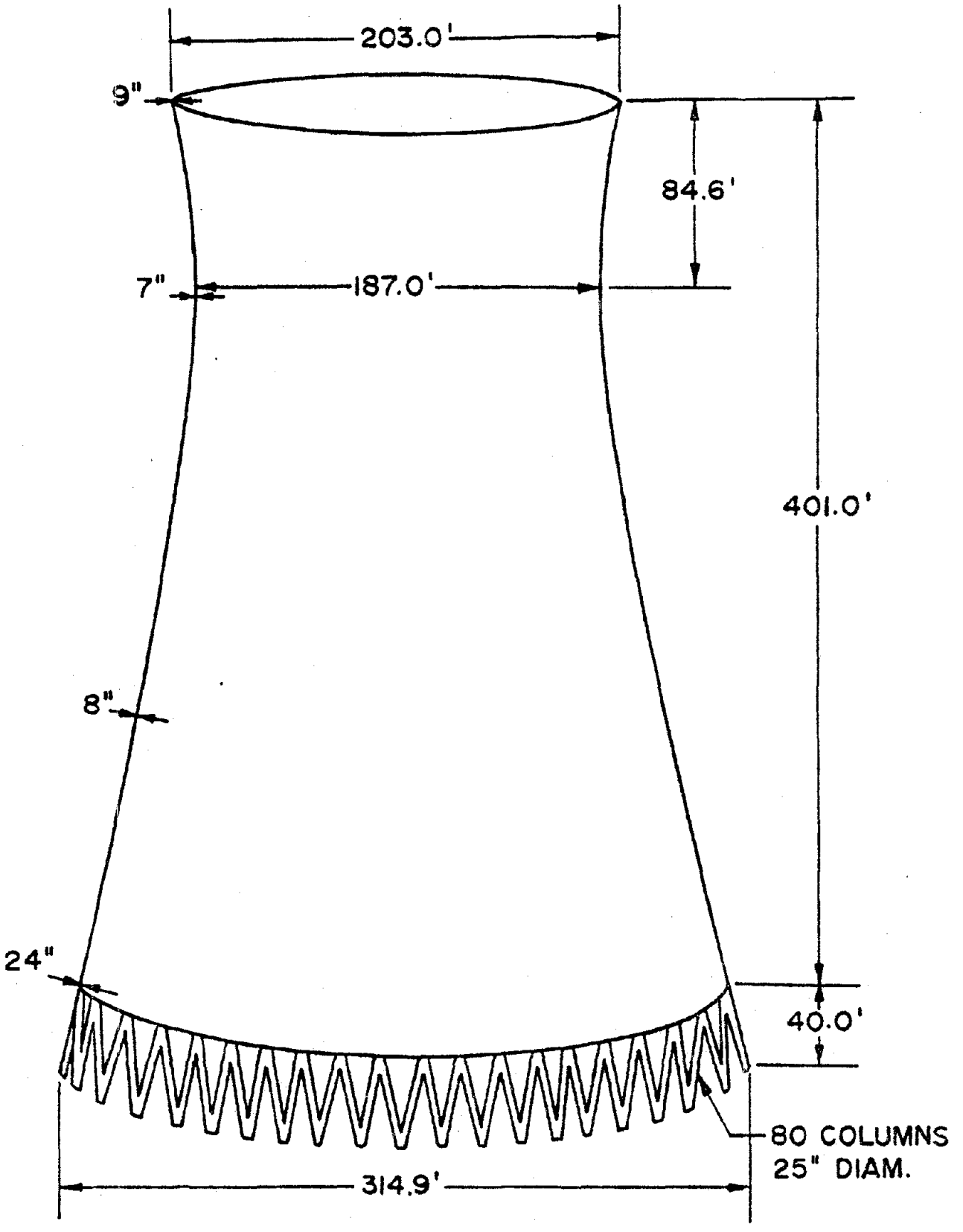

Fig. 1. The Hyperbolic Cooling Tower in the TVA Steam Generating Power Plant, Unit #3, Paradise, Kentucky.

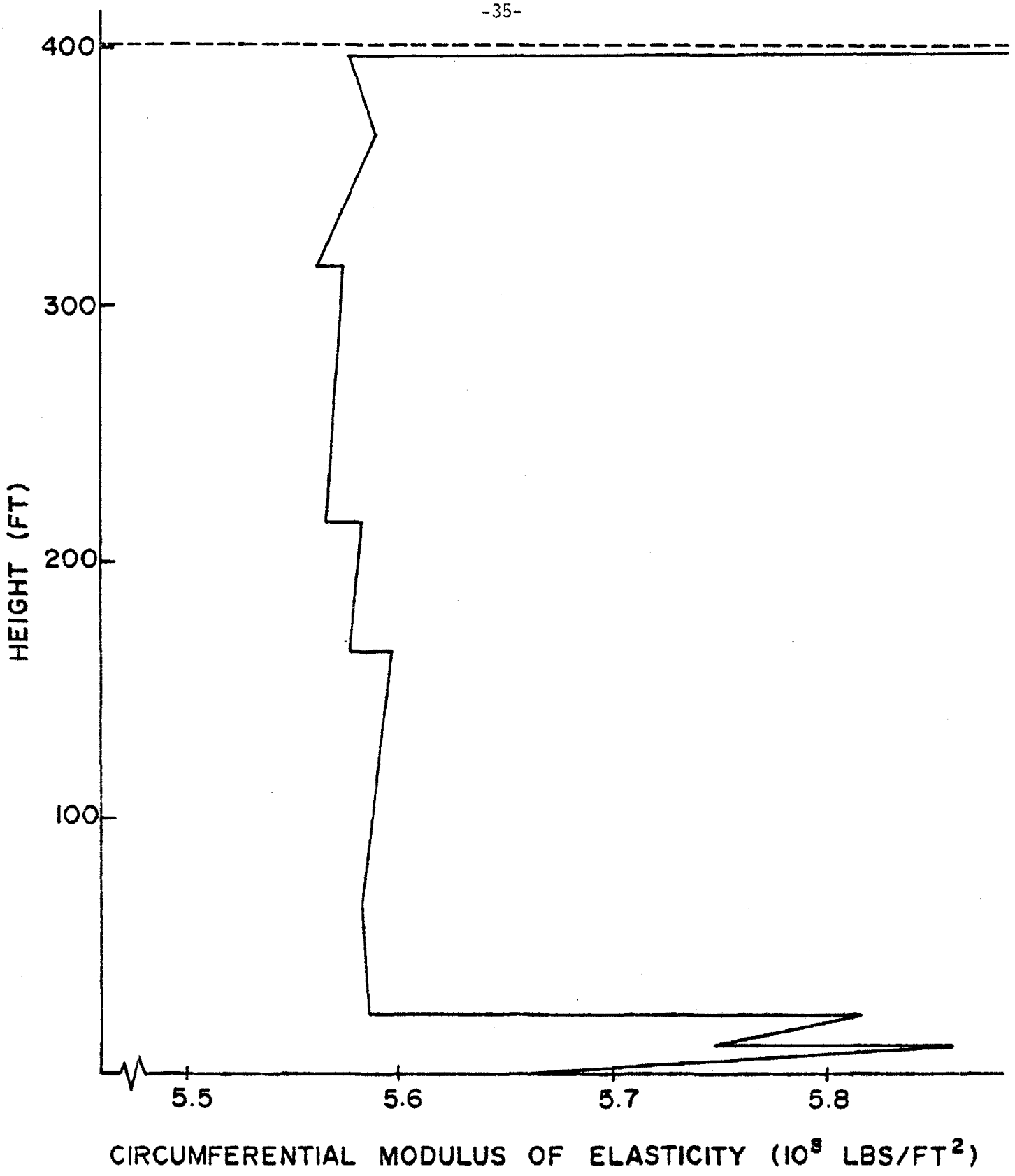

Fig. 2. The Distribution of Equivalent Modulus of Elasticity for the Circumferential Reinforcements Along the Meridional Direction.

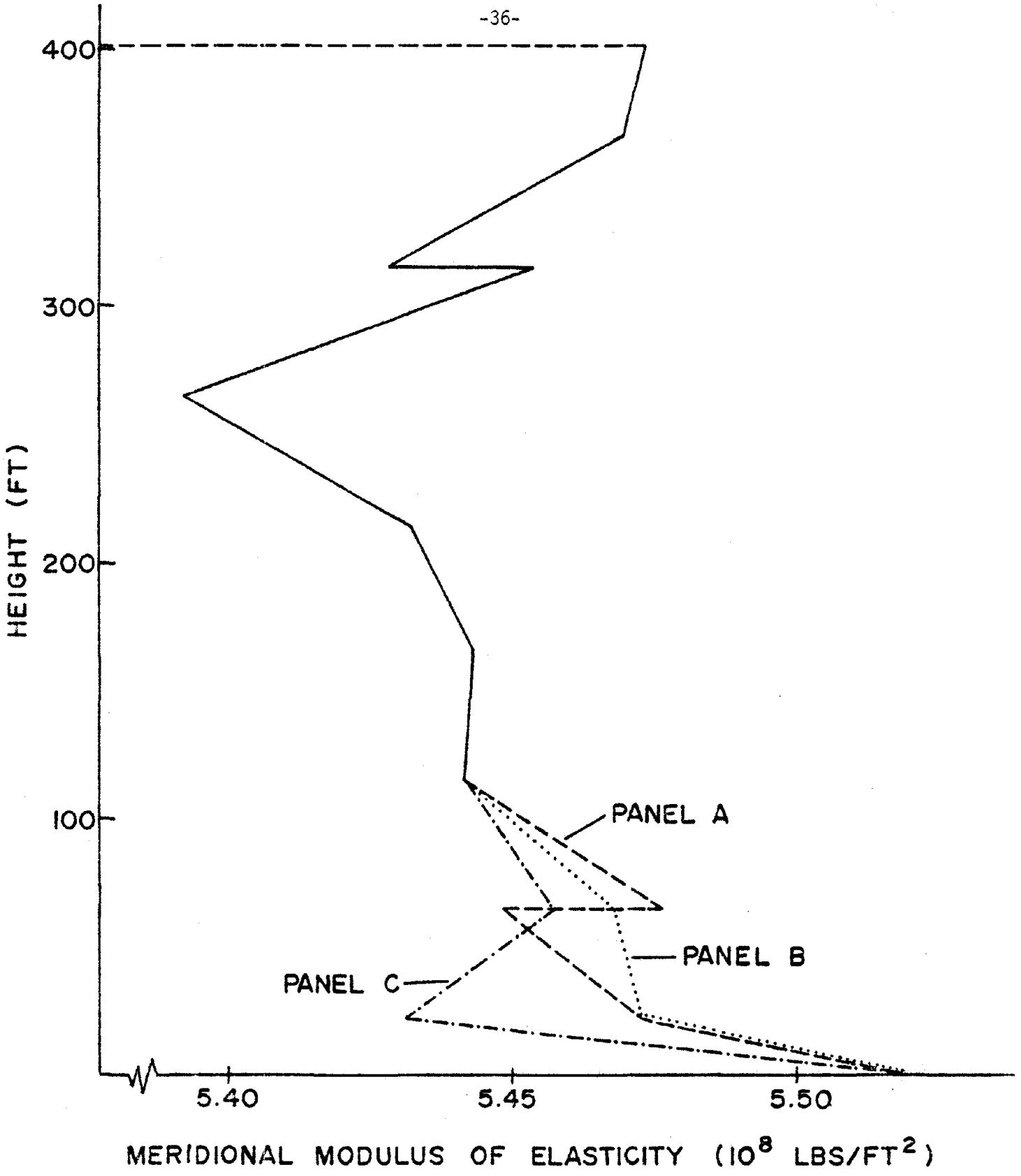

Fig. 3. The Distribution of Equivalent Modulus of Elasticity for the Meridional Reinforcements Along the Meridional Direction.

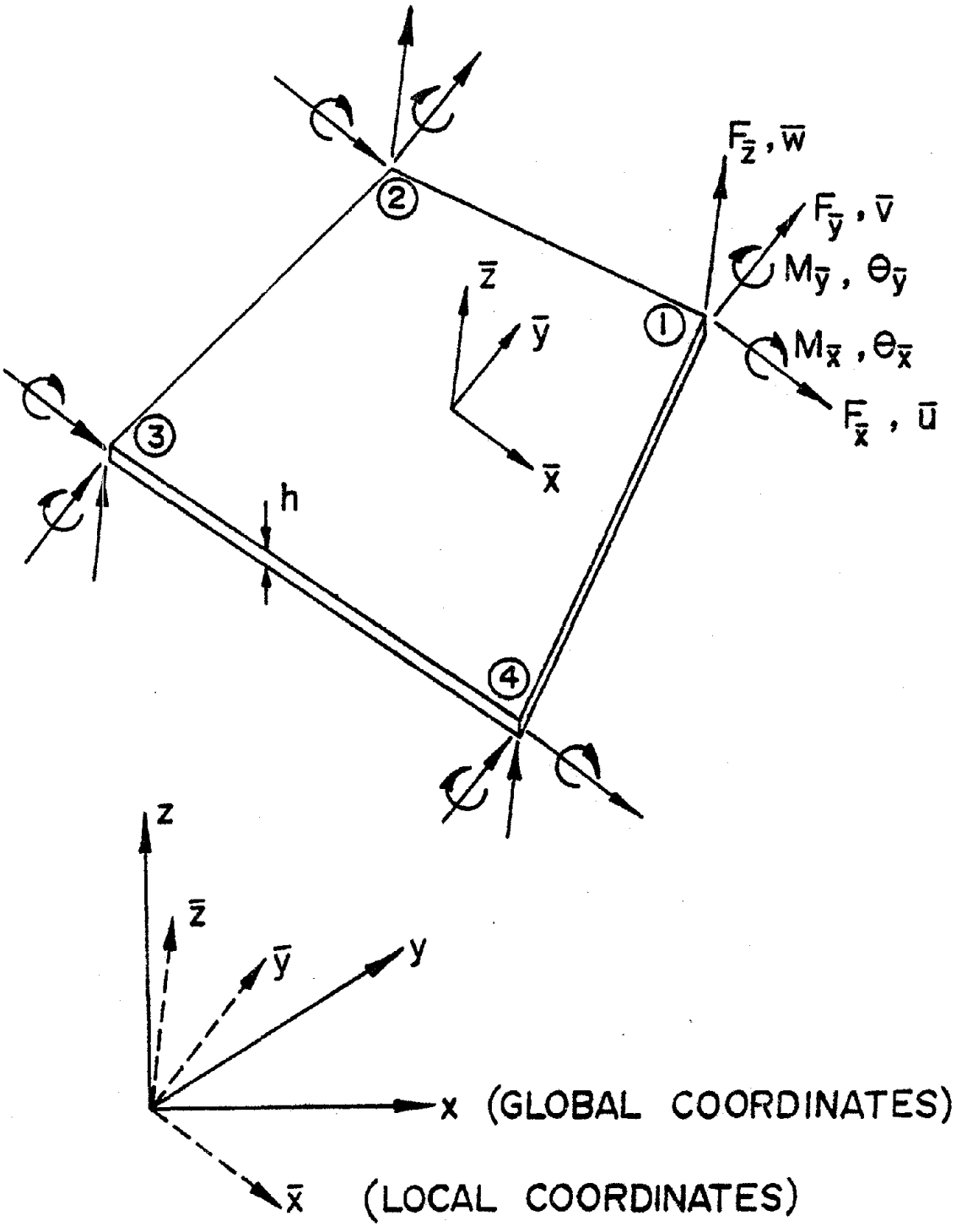

Fig. 4. A Quadrilateral Plate Finite Element in the Three-Dimensional Space.

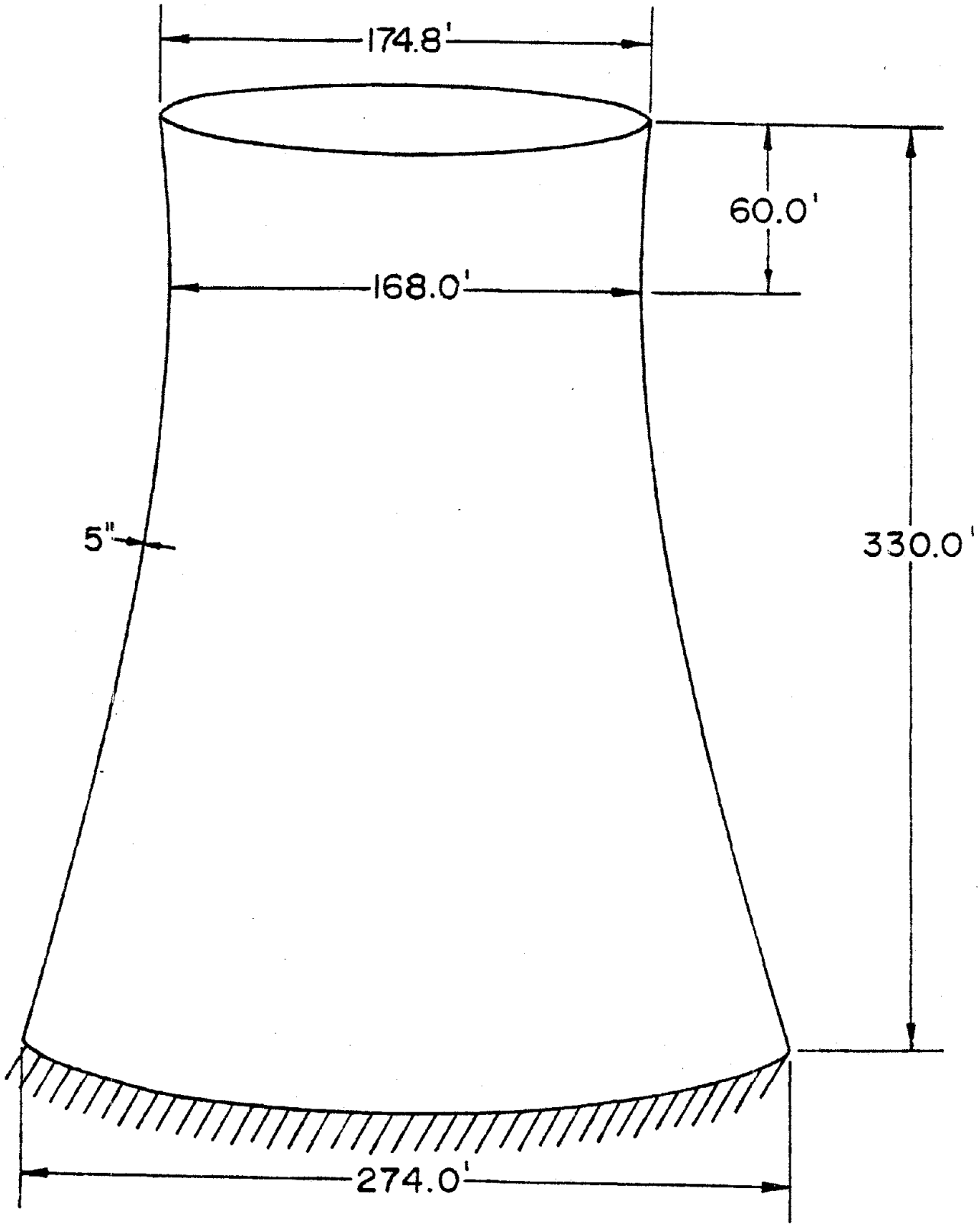

Fig. 5. An Example of a Reinforced Concrete Cooling Tower with Base Fixed.

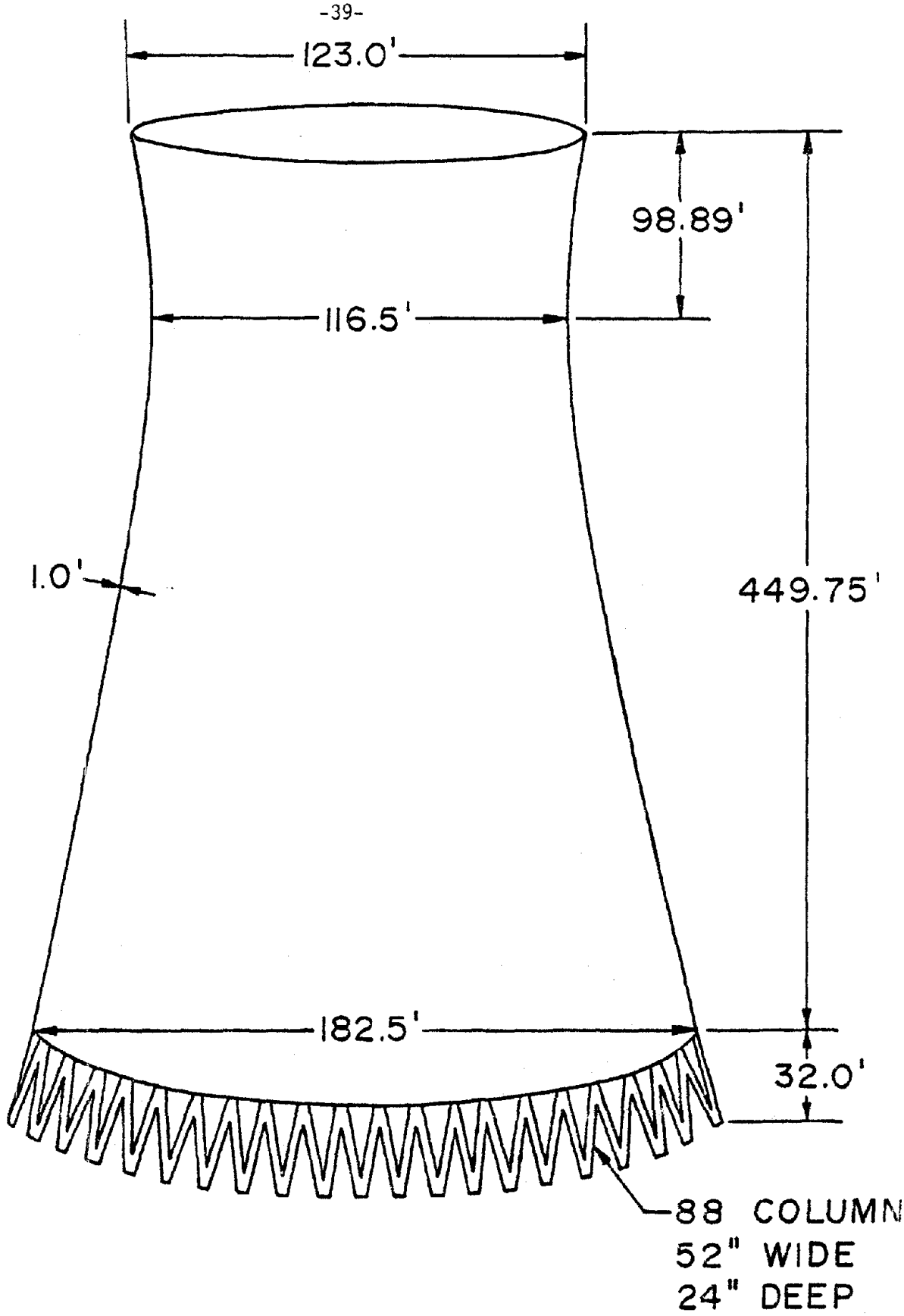

Fig. 6. An Example of a Reinforced Concrete Cooling Tower with Discrete Column Supports.

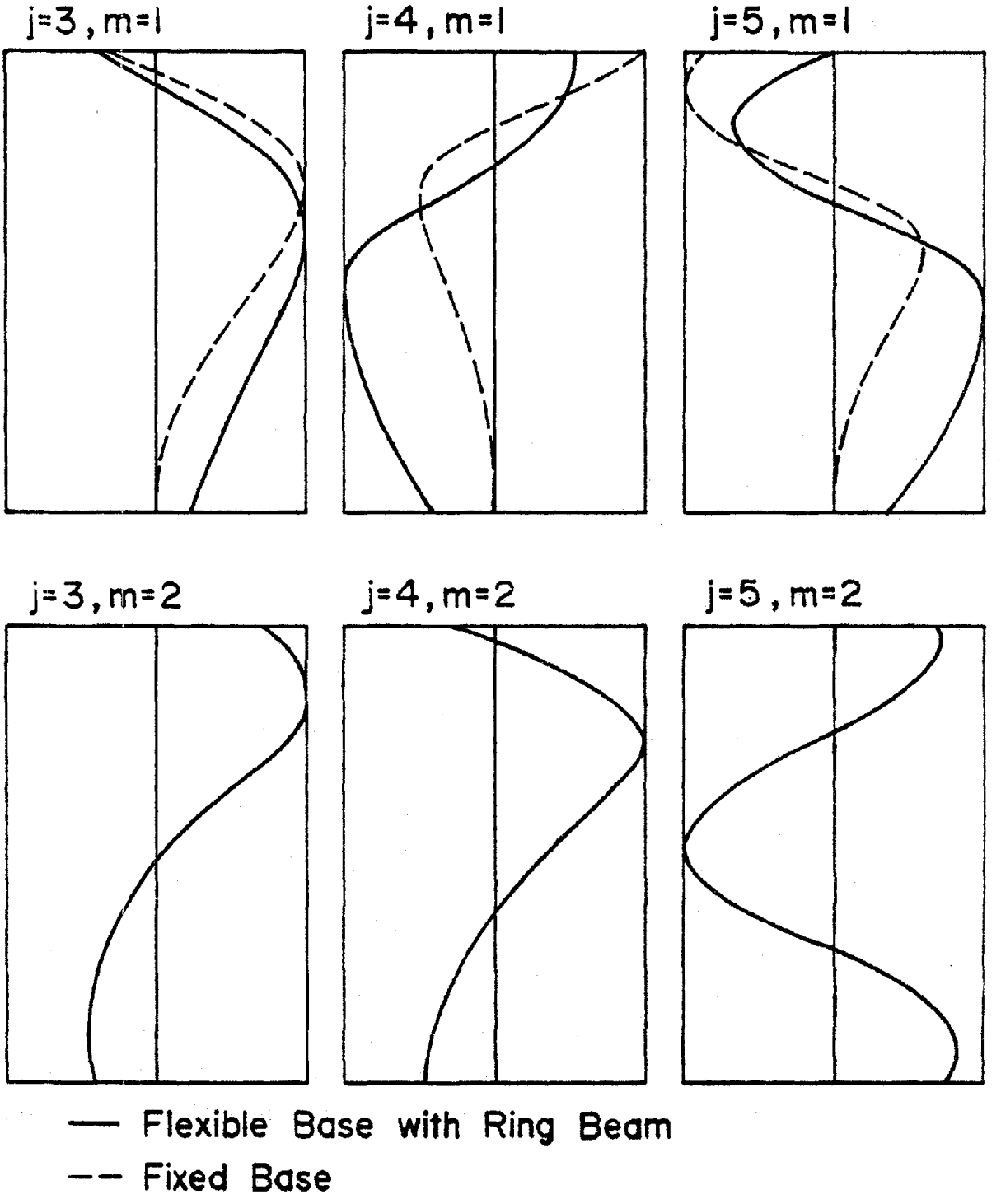

Fig. 7. The Radial Deflection of a Meridional Line for Several Modes of the Paradise Cooling Tower (j = Circumferential Mode Number, m = meridional mode number).

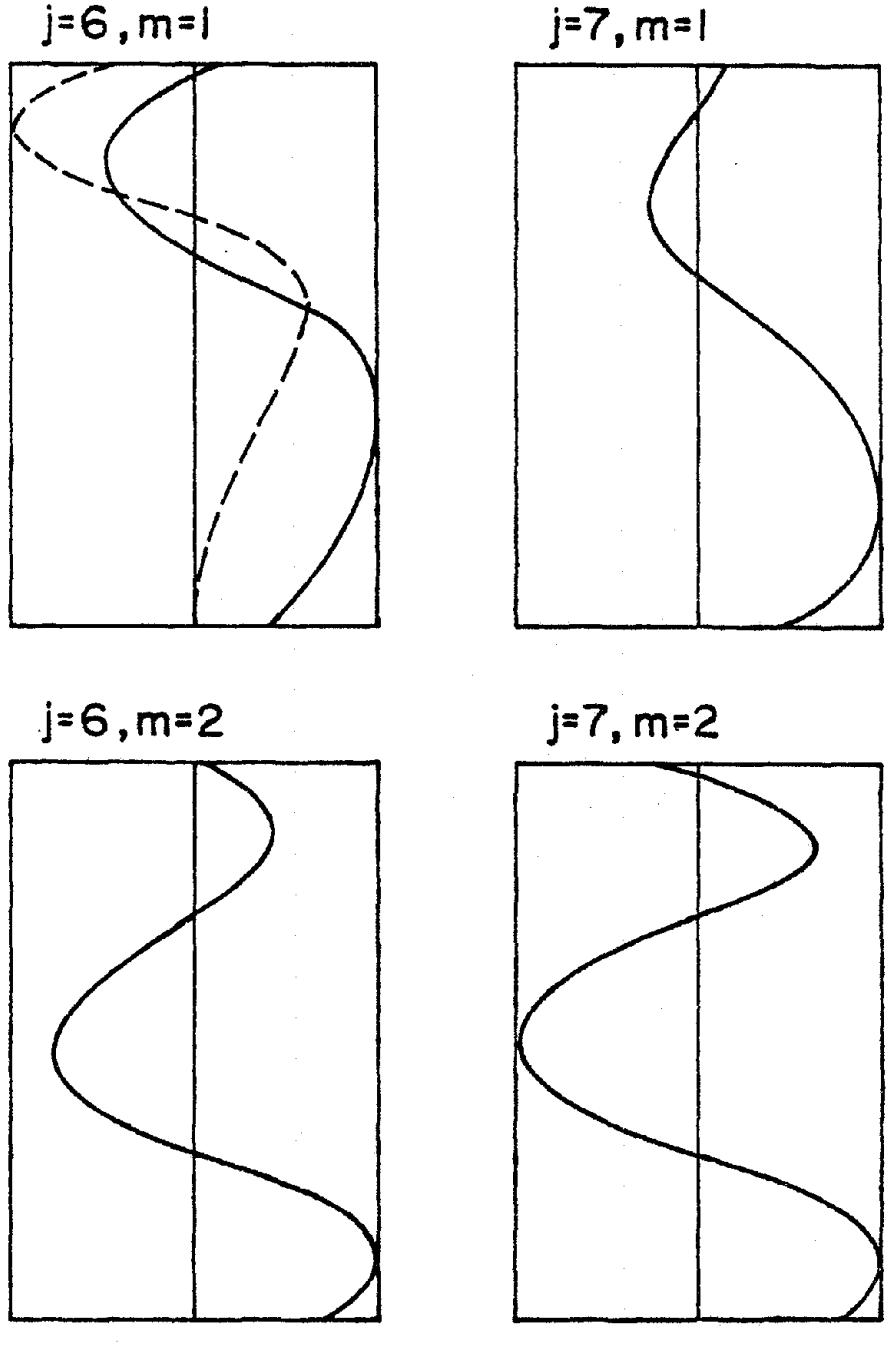

Fig. 7. (cont.) The Radial Deflection of a Meridional Line for Several Modes of the Paradise Cooling Tower (j = Circumferential Mode Number, m = meridional mode number).

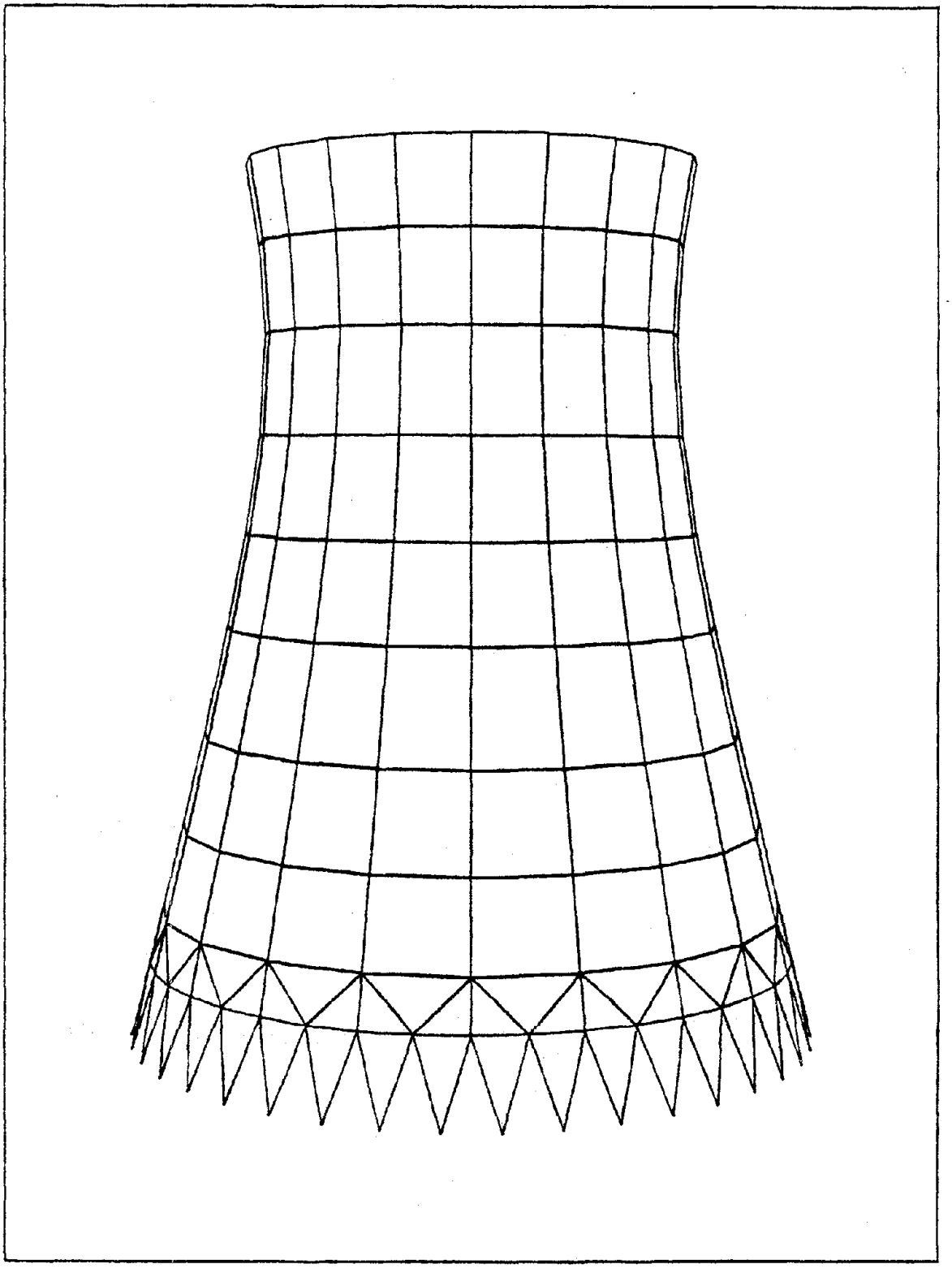

Fig. 8. The Finite Element Modeling of the Paradise Cooling Tower (9 x 10 Half-Shell Model with Two Beam Elements Per Column).

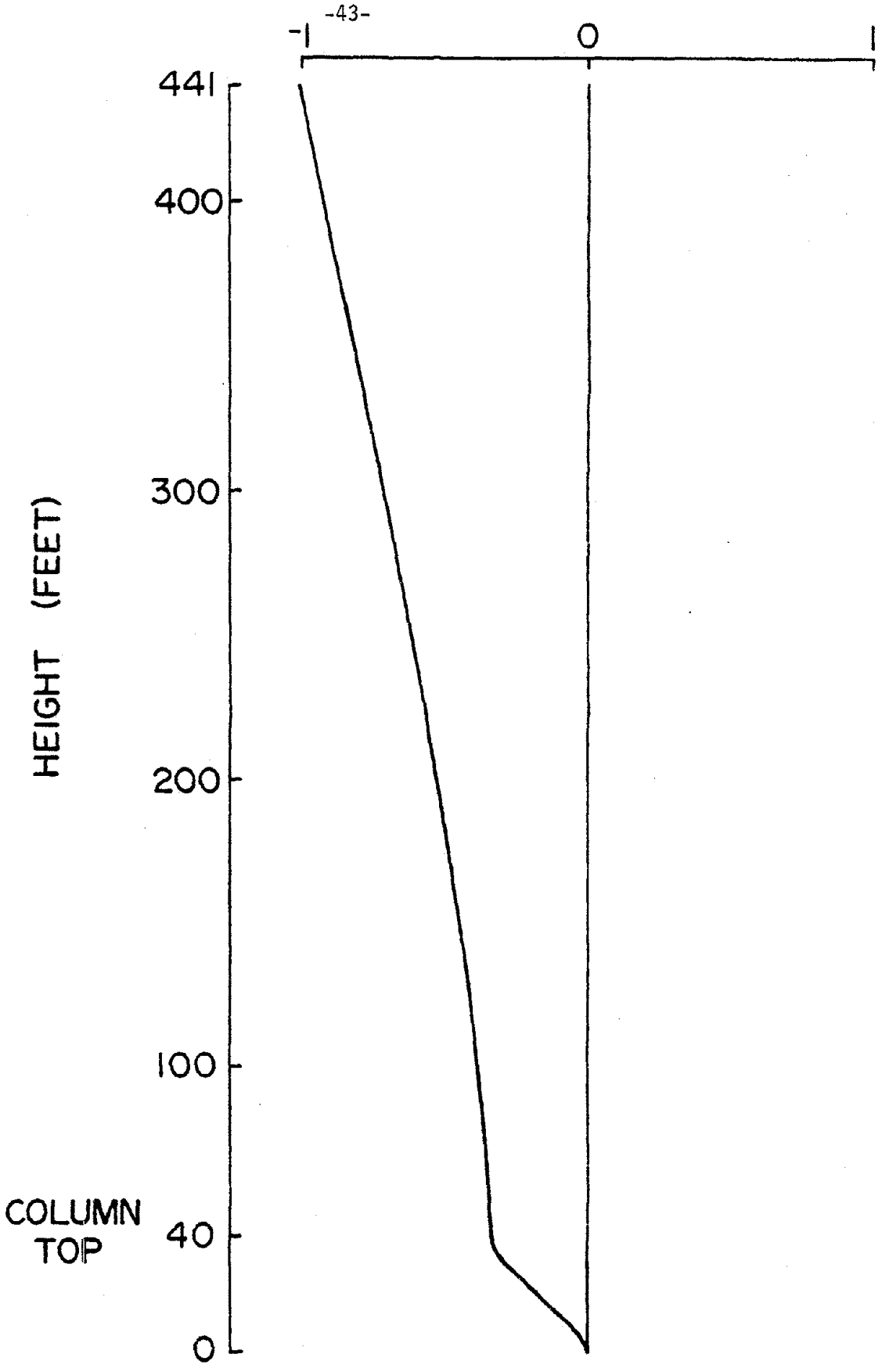

Fig. 9. The Radial Deflection of a Meridional Line in the First Eccentric Mode of the Paradise Cooling Tower.

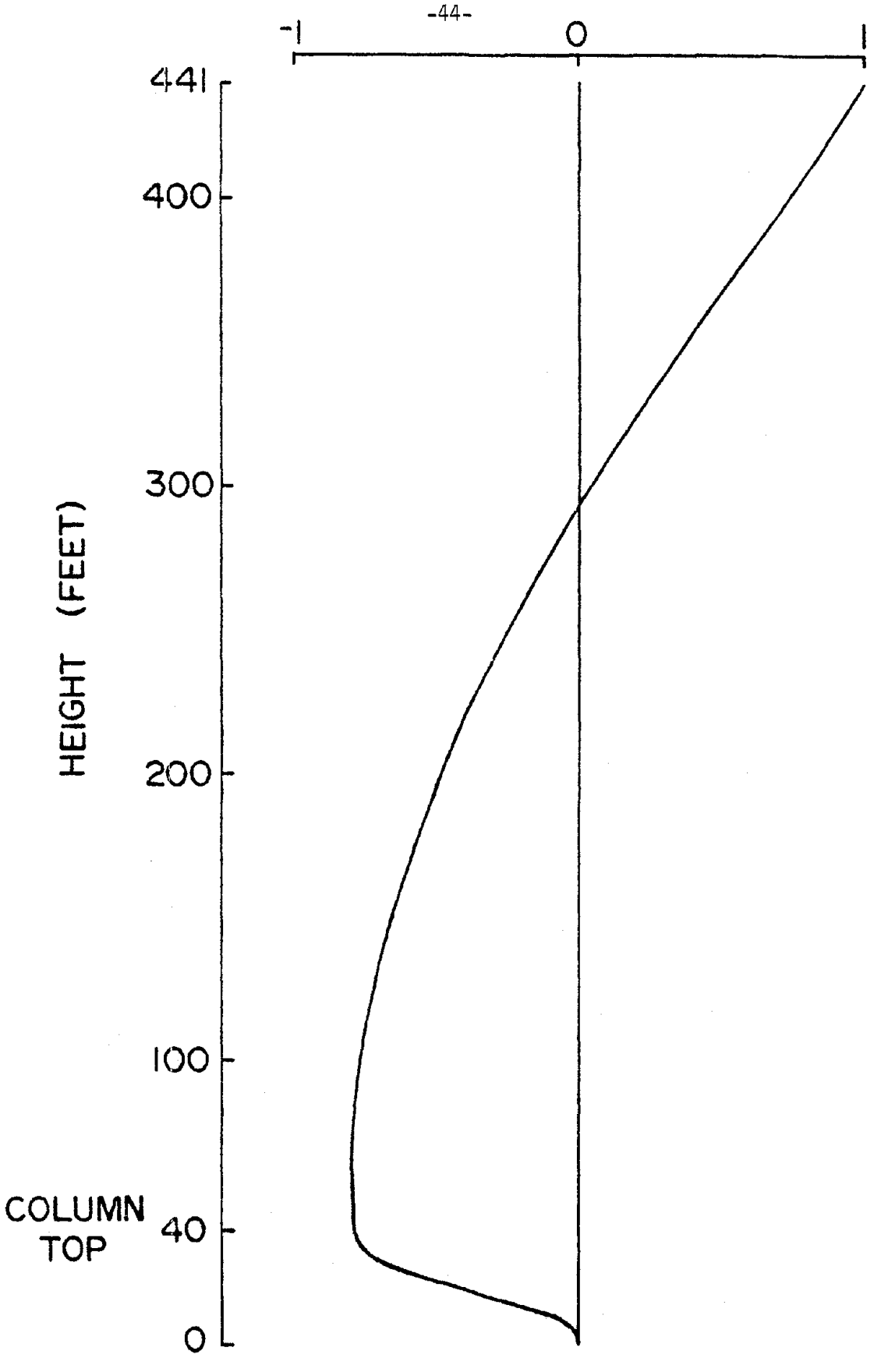

Fig. 10. The Radial Deflection of a Meridional Line in the Second Eccentric Mode.

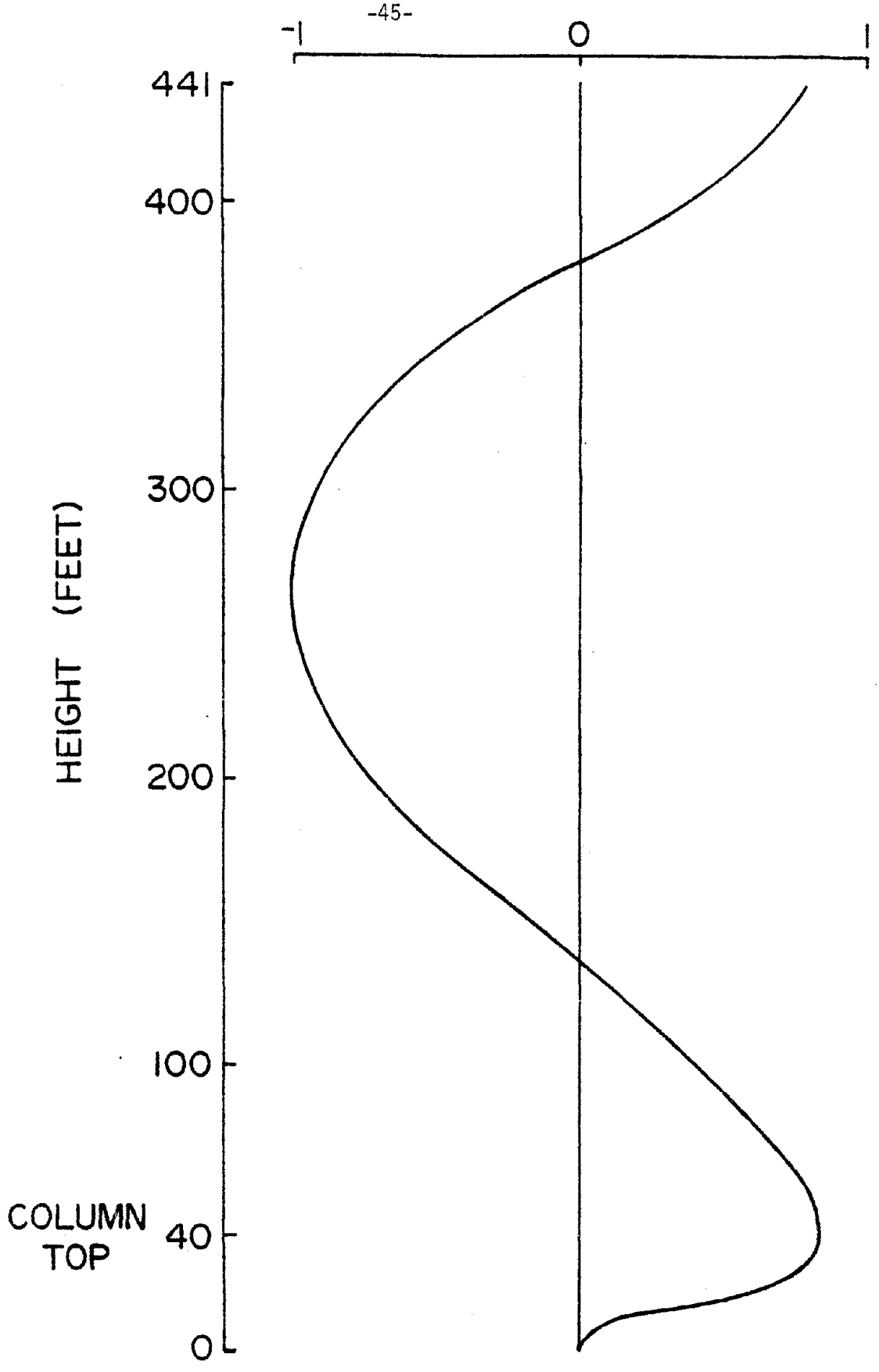

Fig. 11. The Radial Deflection of a Meridional Line in the Third Eccentric Mode.

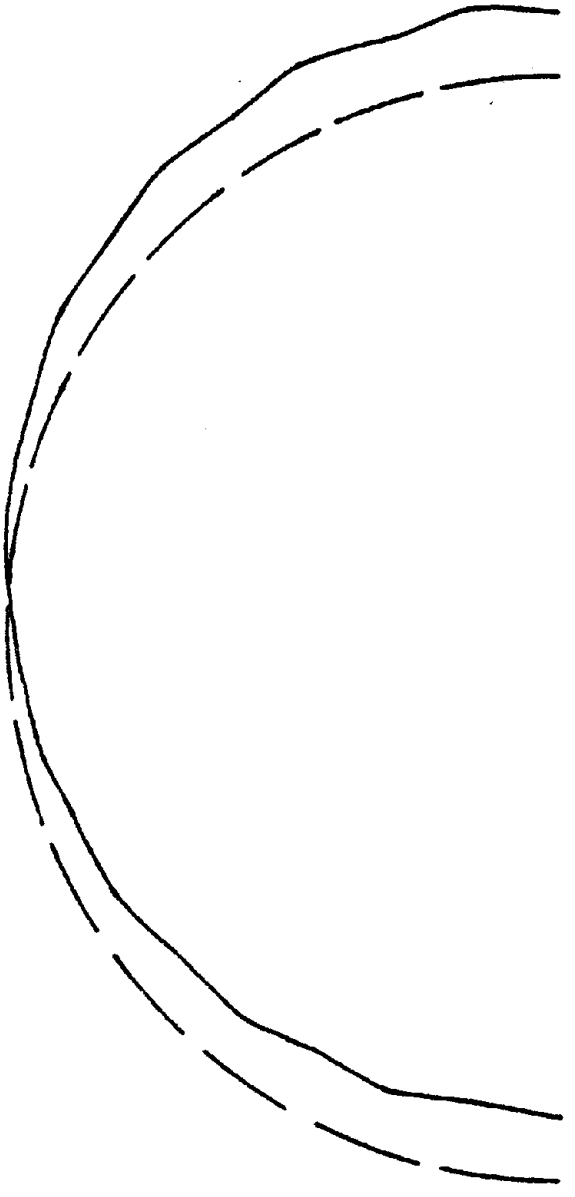

Fig. 12. The Circumferential Deflection at the Shell Base of the First Eccentric Mode.

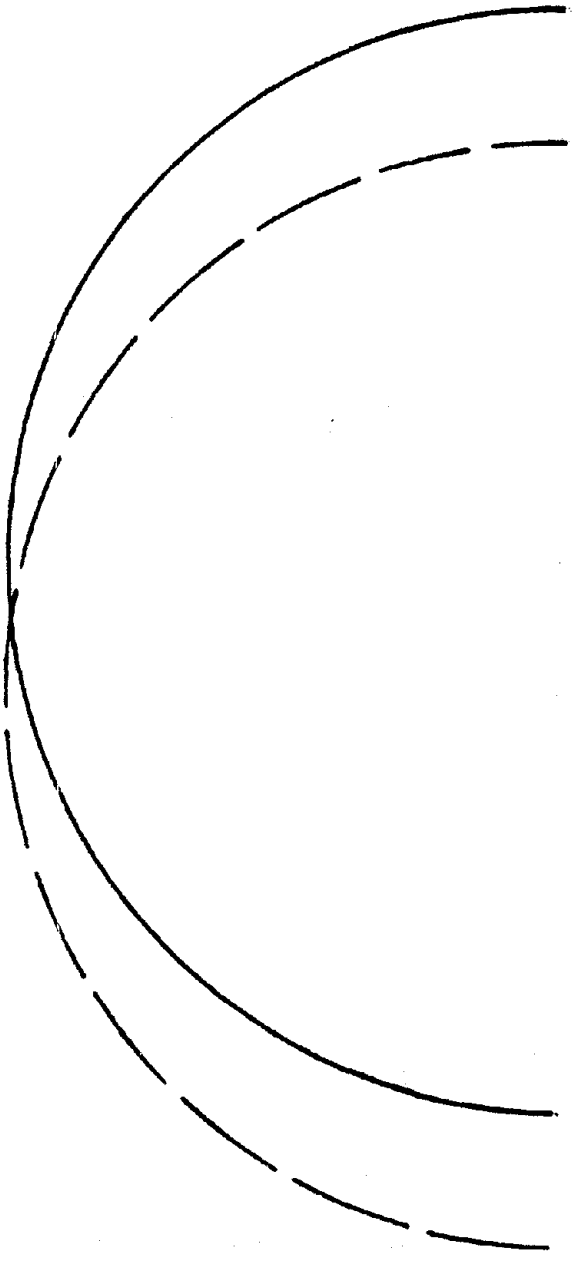

Fig. 13. The Circumferential Deflection at the Shell Base of the Second Eccentric Mode.

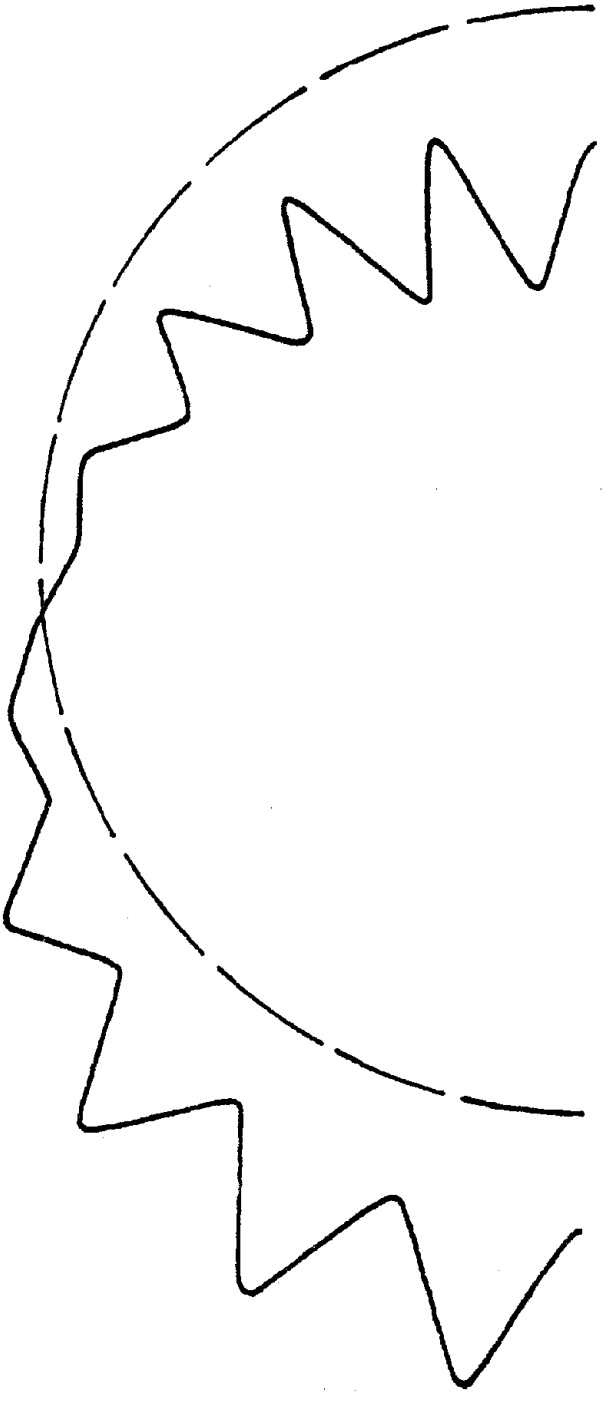

Fig. 14. The Circumferential Deflection at the Shell Base of the Third Eccentric Mode.

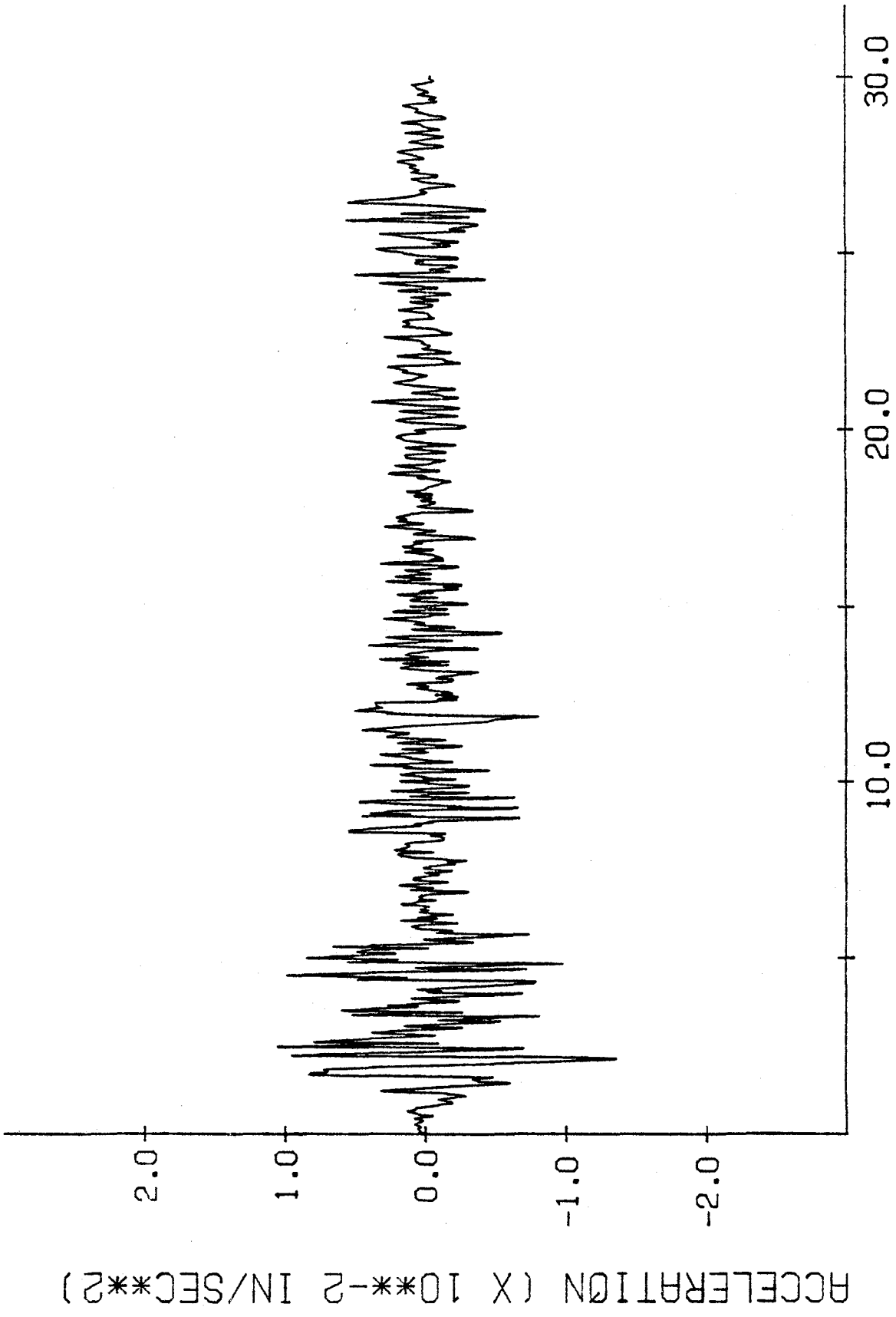

Fig. 15. The North-South Acceleration Component of the 1940 El Centro Earthquake.

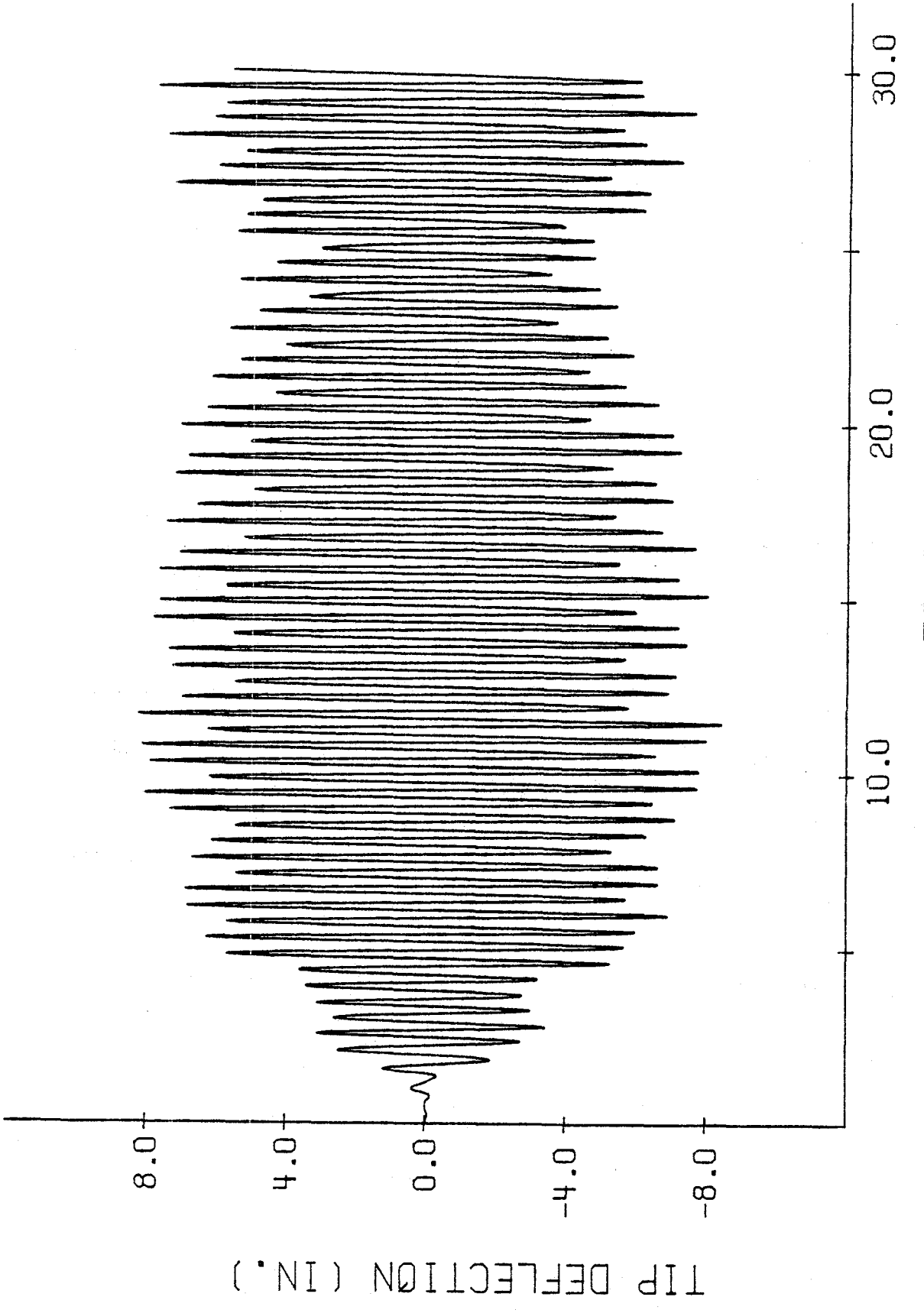

Fig. 16. The Time-History Response of Shell Tip Deflection at $\theta = 0°$ for the Undamped Case.

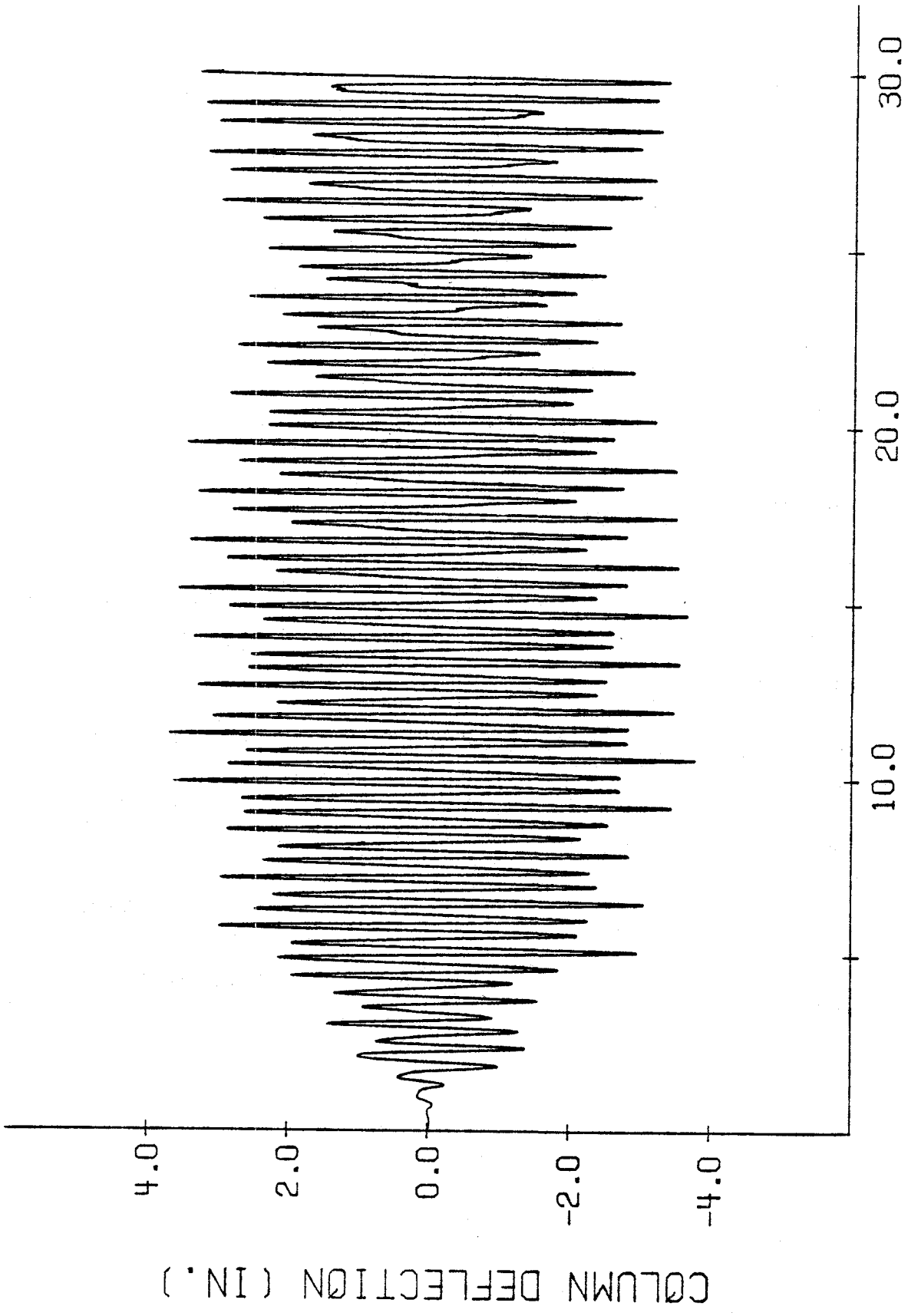

Fig. 17. The Time-History Response of Column Top Deflection at $\theta = 0°$ for the Undamped Case.

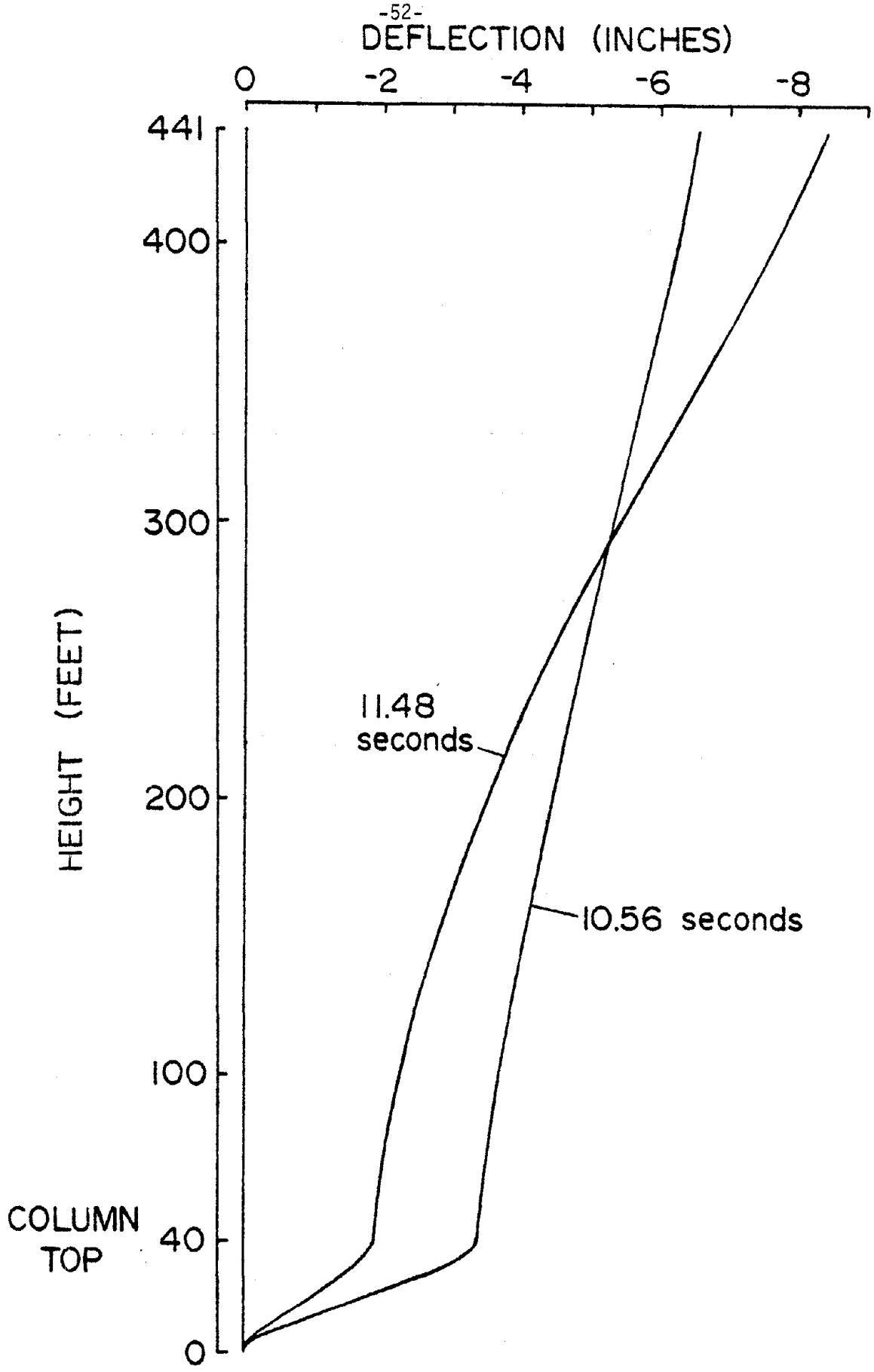

Fig. 18. The Radial Deflection of the Meridional Line at $\theta = 0°$ at the time of Maximum Shell Tip Deflection ($t = 11.48$ seconds) and the Time of Maximum Column Top Deflection ($t = 10.56$ seconds).

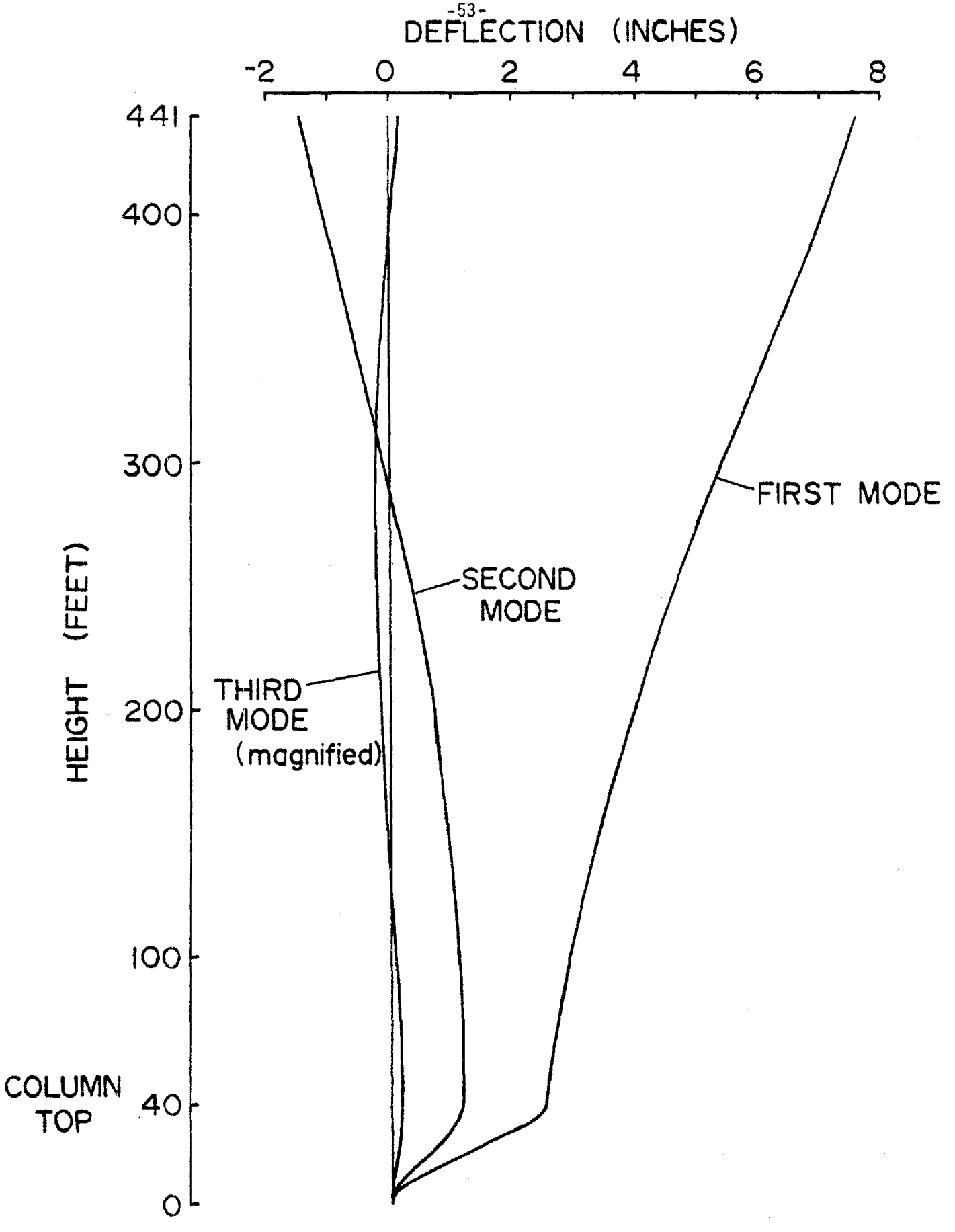

Fig. 19. Maximum Individual Undamped Radial Deflections of the First Three Eccentric Modes from the Spectral Analysis (with the Third Mode Magnified Ten Times).

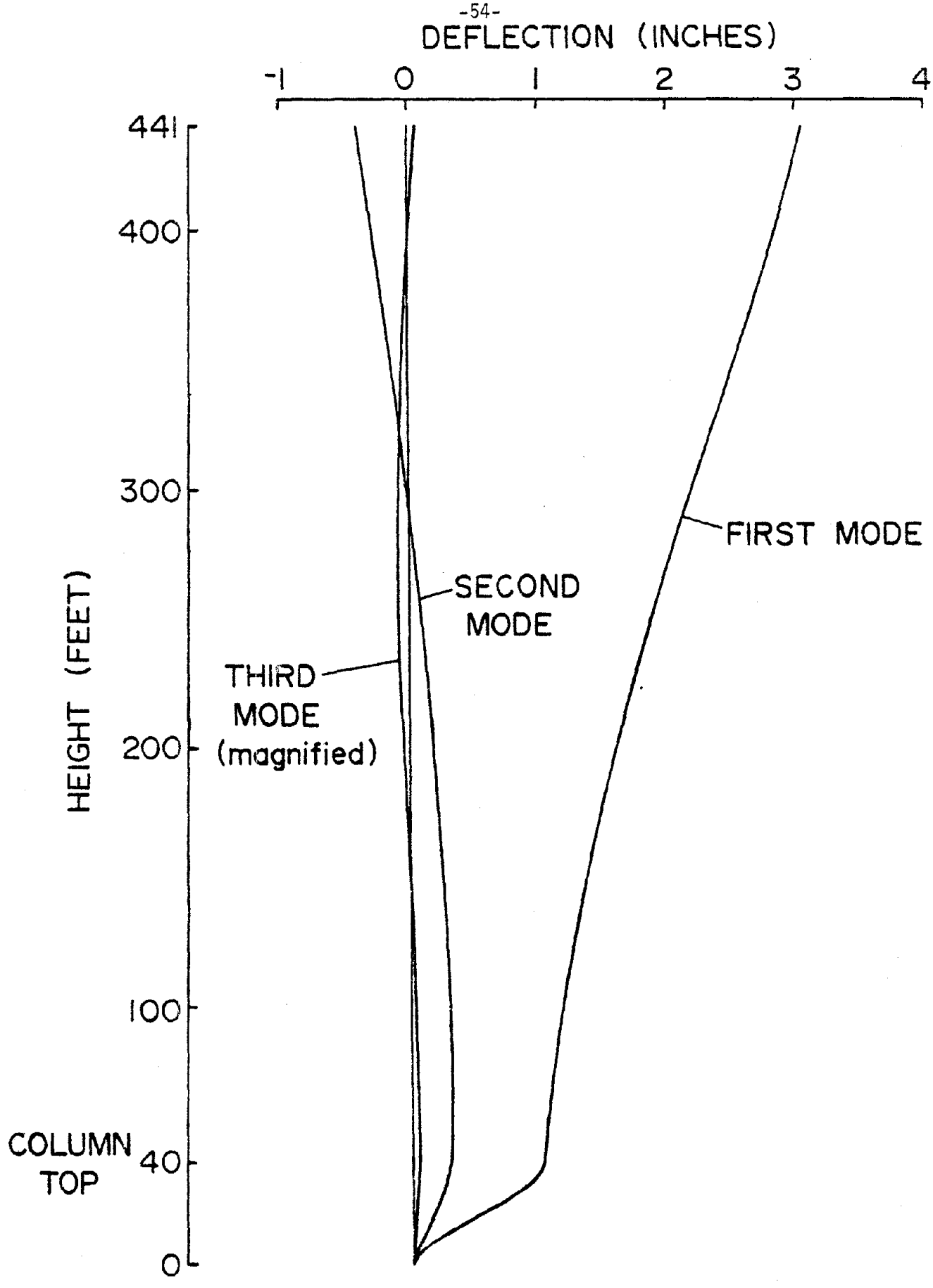

Fig. 20. Maximum Individual Radial Deflections of the First Three Eccentric Modes with Four Percent Damping from the Spectral Analysis (with the Third Mode Magnified Ten Times).

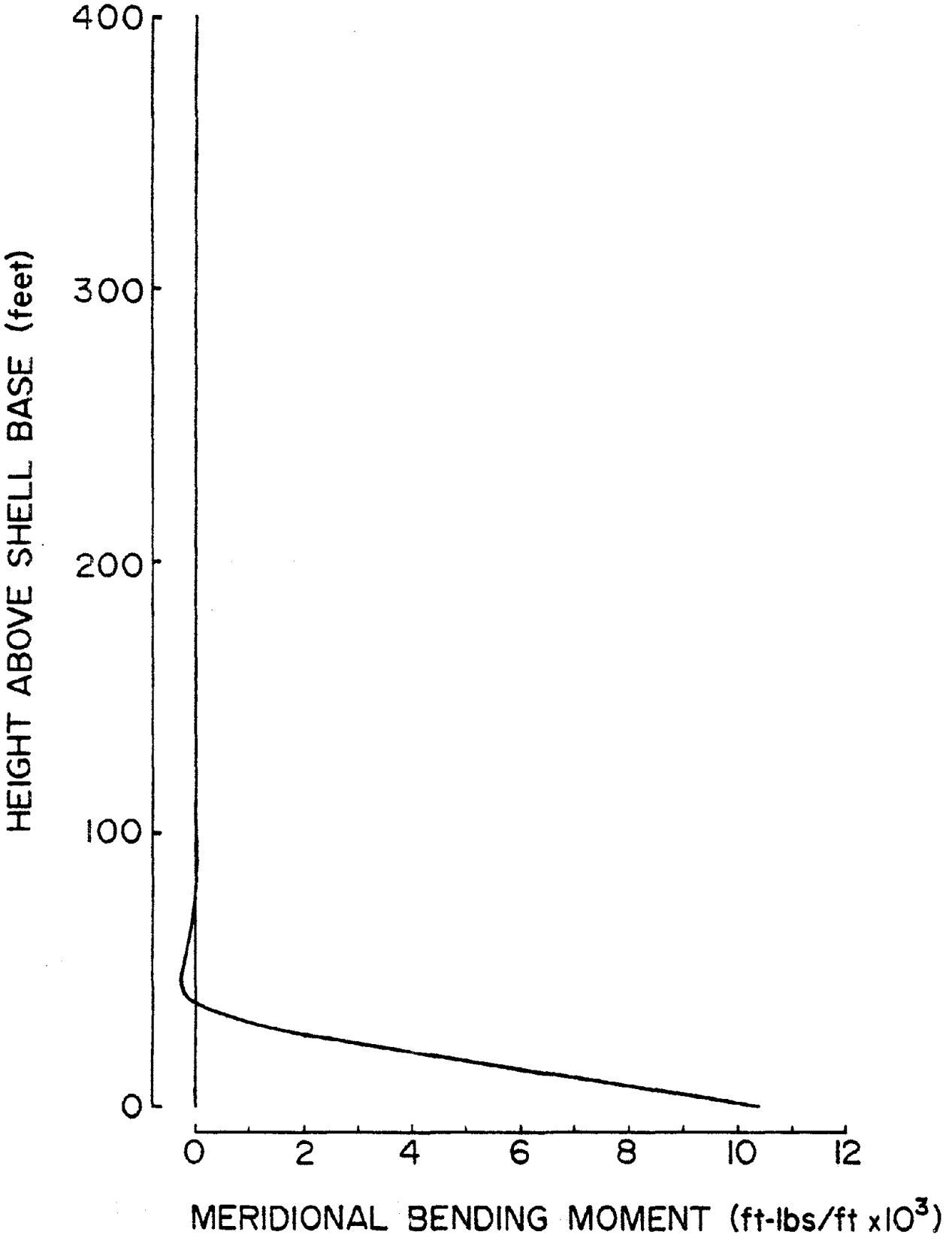

Fig. 21. Longitudinal Distribution of Meridional Bending Moment at $\theta = 0°$.

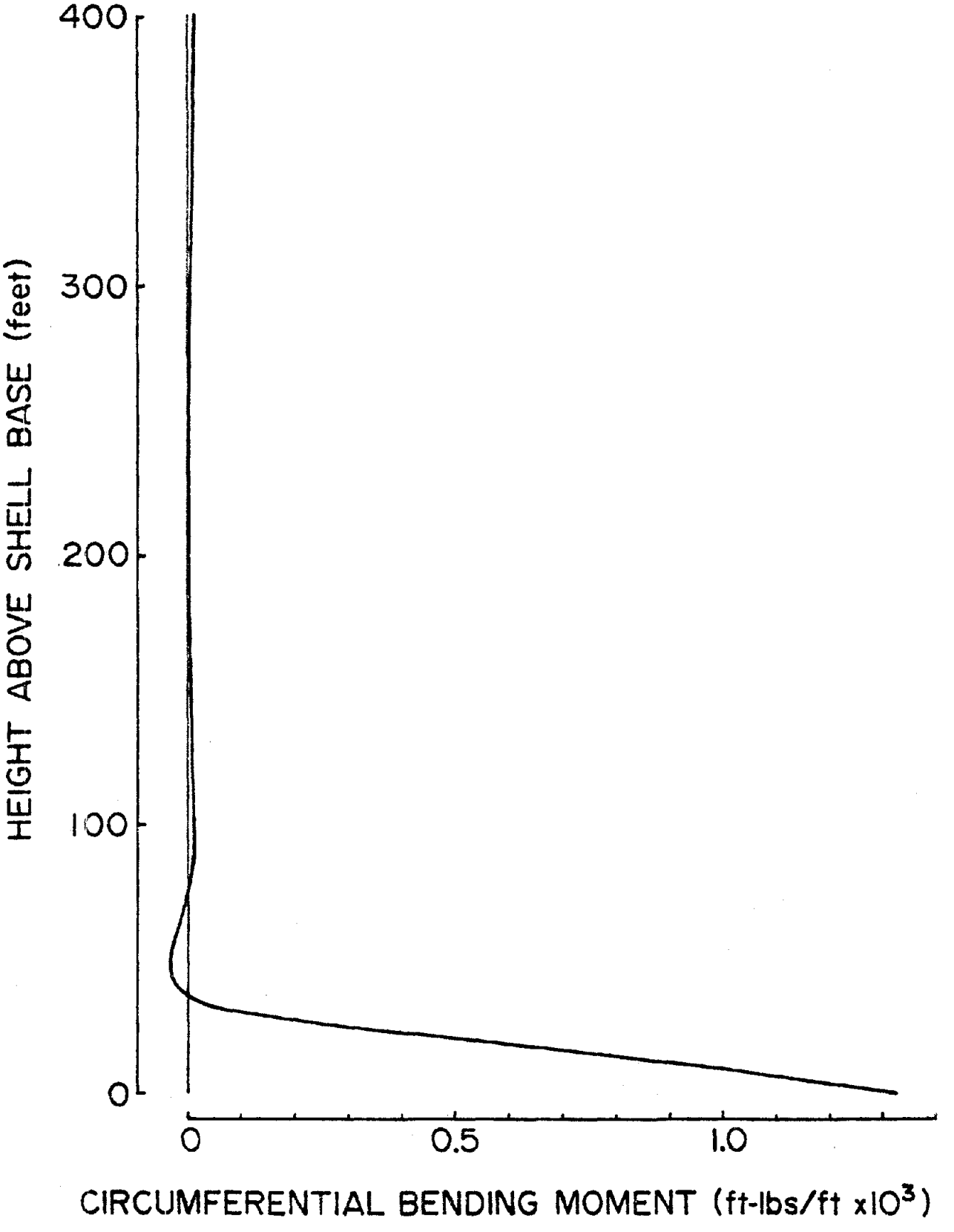

Fig. 22. Longitudinal Distribution of Circumferential Bending Moment at $\theta = 0°$.

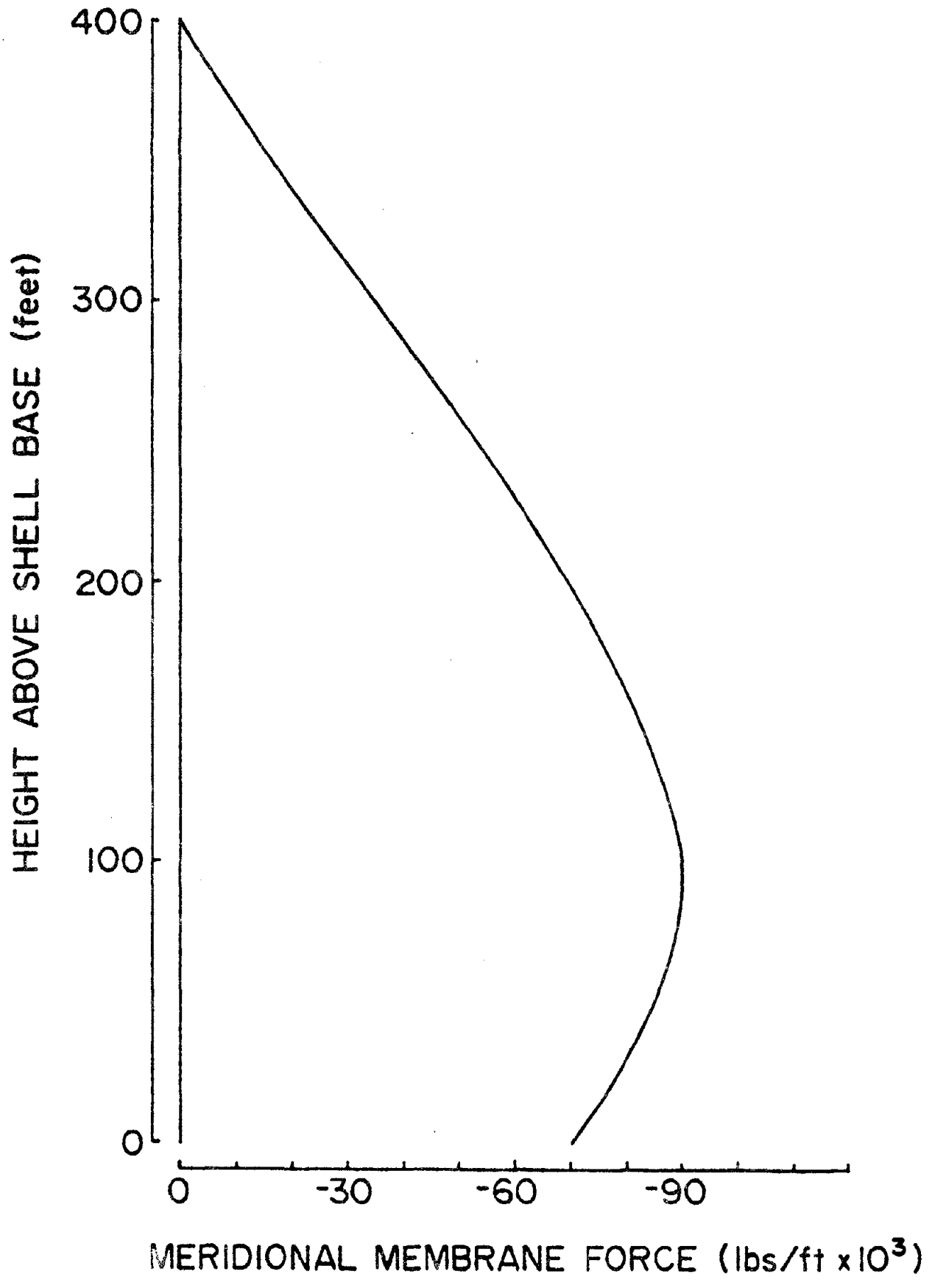

Fig. 23. Longitudinal Distribution of Meridional Membrane Force at $\theta = 180°$.

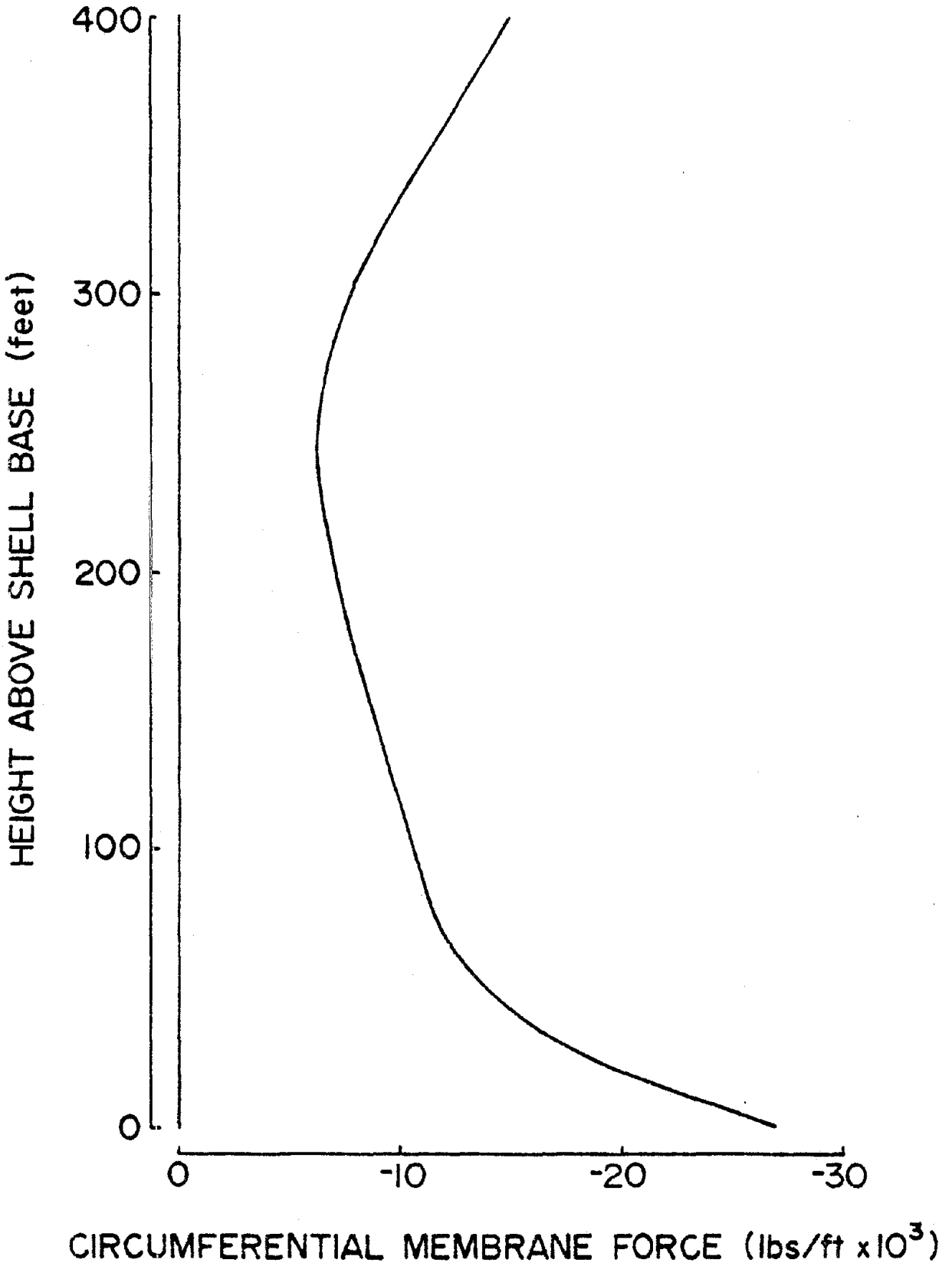

Fig. 24. Longitudinal Distribution of Circumferential Membrane Force at $\theta = 0°$.

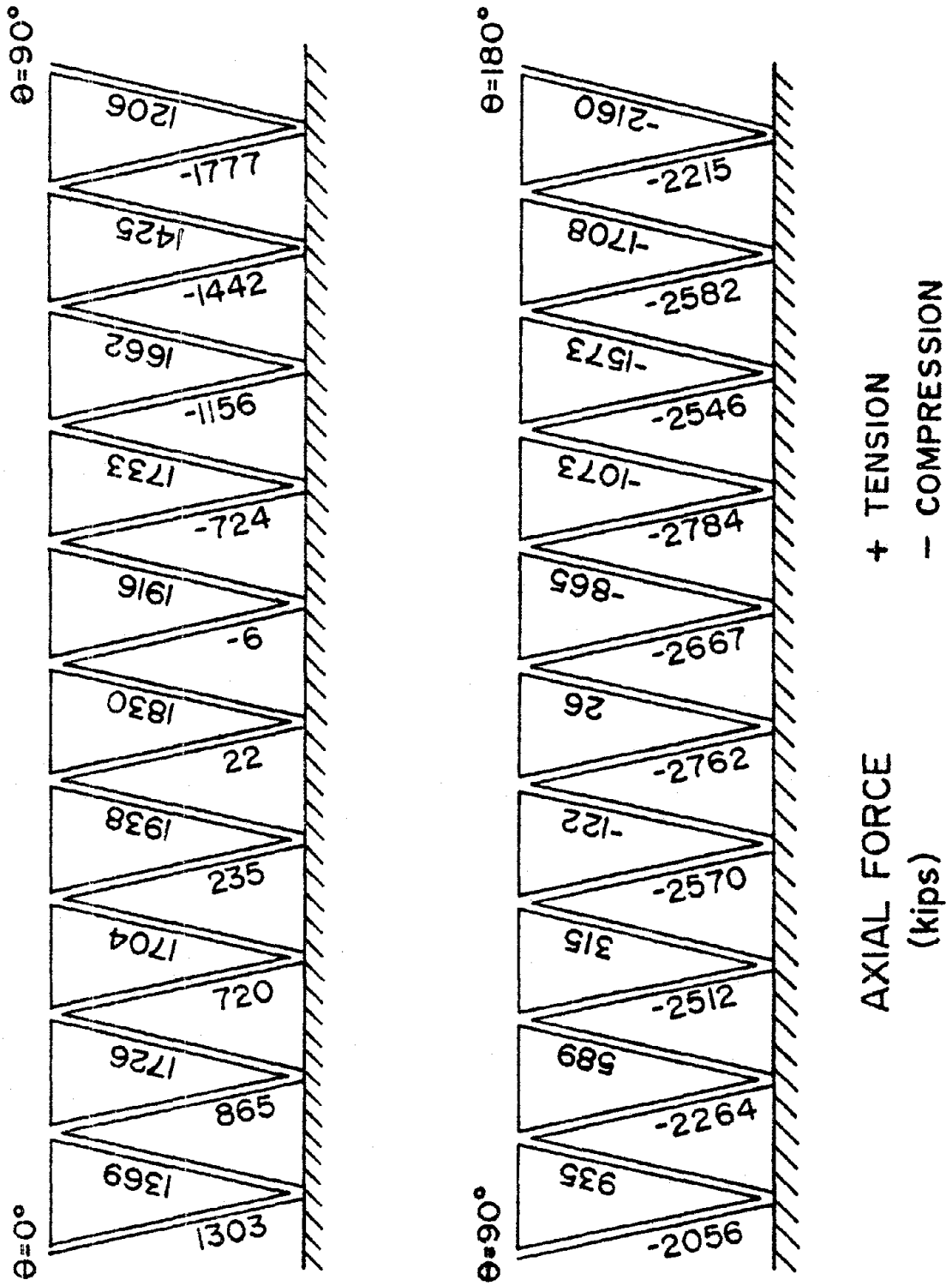

Figure 25. Average Axial Force in the Supporting Columns.

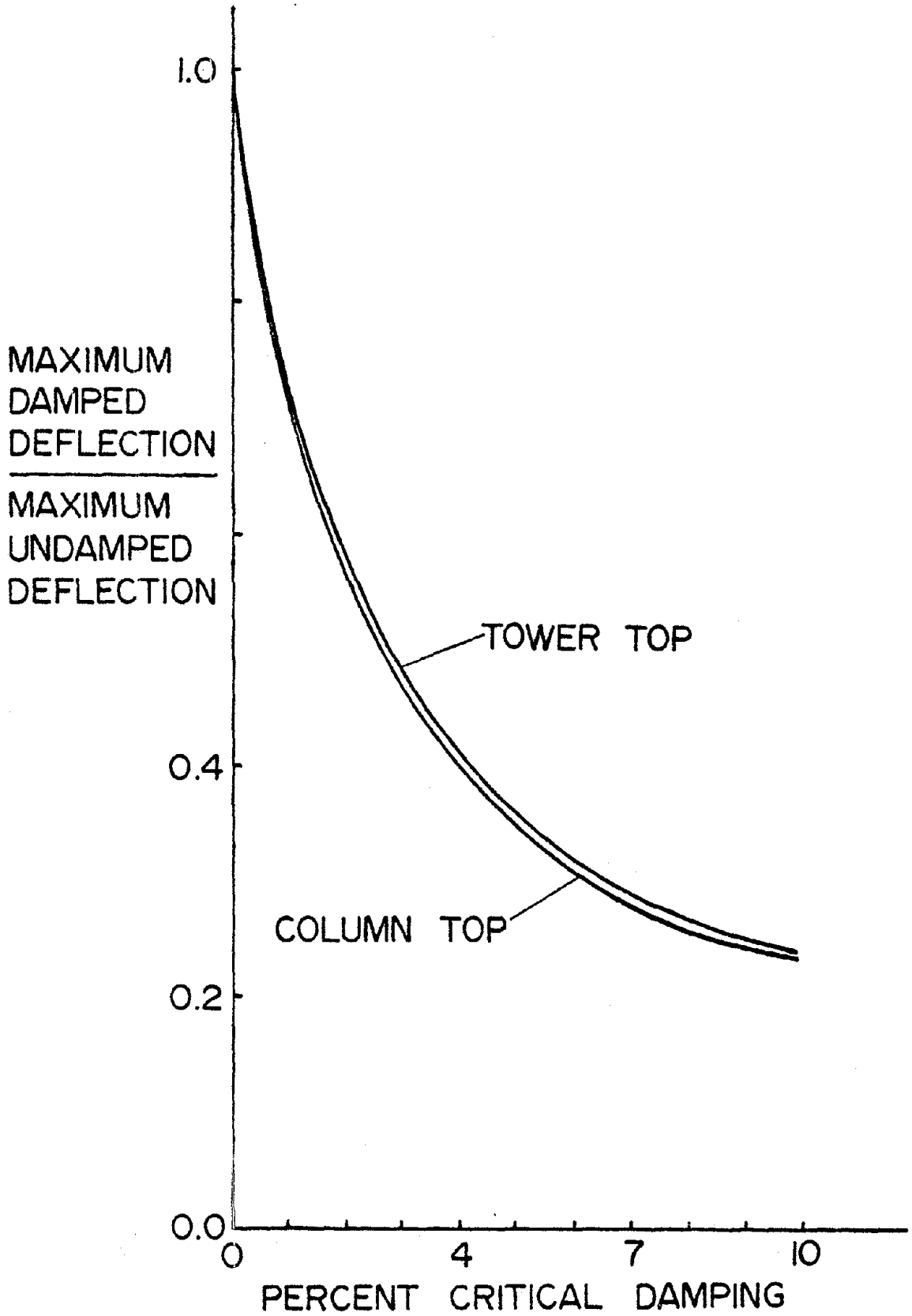

Variations of Maximum Tip Deflection Ratio and Maximum Column Top Deflection Ratio versus Damping Coefficient.